J. Plasma Physics (2001), *vol.* 66, *part* 3, *pp.* 167–212. © 2001 Cambridge University Press
DOI: 10.1017/S0022377801001283 Printed in the United Kingdom

Parametric instabilities and wave coupling in Alfvén simple waves

G. M. WEBB,[1] A. R. ZAKHARIAN,[2] M. BRIO[3] and G. P. ZANK[4]

[1]Lunar and Planetary Laboratory, University of Arizona, Tucson, AZ 85721, USA
[2]Arizona Center for Mathematical Sciences, University of Arizona, Tucson AZ 85721, USA
[3]Department of Mathematics, University of Arizona, Tucson, AZ 85721, USA
[4]Bartol Research Institute, University of Delaware, Newark, DE 19716, USA

(Received 11 December 2000 and in revised form 27 April 2001)

Abstract. A wave coupling formalism for magnetohydrodynamic (MHD) waves in a non-uniform background flow is used to study parametric instabilities of the large-amplitude, circularly polarized, simple plane Alfvén wave in one Cartesian space dimension. The large-amplitude Alfvén wave (the pump wave) is regarded as the background flow, and the seven small-amplitude MHD waves (the backward and forward fast and slow magnetoacoustic waves, the backward and forward Alfvén waves, and the entropy wave) interact with the pump wave via wave coupling coefficients that depend on the gradients and time dependence of the background flow. The dispersion equation for the waves $D(k,\omega) = 0$ obtained from the wave coupling equations reduces to that obtained by previous authors. The general solution of the initial value problem for the waves is obtained by Fourier and Laplace transforms. The dispersion function $D(k,\omega)$ is a fifth-order polynomial in both the wavenumber k and the frequency ω. The regions of instability and the neutral stability curves are determined. Instabilities that arise from solving the dispersion equation $D(k,\omega) = 0$, both in the form $\omega = \omega(k)$, where k is real, and in the form $k = k(\omega)$, where ω is real, are investigated. The instabilities depend parametrically on the pump wave amplitude and on the plasma beta. The wave interaction equations are also studied from the perspective of a single master wave equation, with multiple wave modes, and with a source term due to the entropy wave. The wave hierarchies for short- and long-wavelength waves of the master wave equation are used to discuss wave stability. Expanding the dispersion equation for the different long-wavelength eigenmodes about $k = 0$ yields either the linearized Korteweg–deVries equation or the Schrödinger equation as the generic wave equation at long-wavelengths. The corresponding short-wavelength wave equations are also obtained. Initial value problems for the wave interaction equations are investigated. An inspection of the double-root solutions of the dispersion equation for k, satisfying the equations $D(k,\omega) = 0$ and $\partial D(k,\omega)/\partial k = 0$ and pinch point analysis shows that the solutions of the wave interaction equations for hump or pulse-like initial data develop an absolute instability. Fourier solutions and asymptotic analysis are used to study the absolute instability.

https://doi.org/10.1017/S0022377801001283 Published online by Cambridge University Press

1. Introduction

Goldstein (1978), Derby (1978) and Jayanti and Hollweg (1993a,b) studied the stability of the large-amplitude, plane, circularly polarized Alfvén wave in magnetohydrodynamics (MHD). The stability of the large-amplitude, circularly polarized Alfvén-like modes in a Hall current plasma were studied by Wong and Goldstein (1986), Terasawa et al. (1986), Hollweg (1994) and Vinas and Goldstein (1991a,b). These instabilities are thought to be important in the development of turbulent Alfvén wave cascades in the solar wind. Hollweg (1994) classifies the instabilities as modulational (if $k \ll k_0$), decay (if $k \gg k_0$) and beat ($k \simeq k_0$) instabilities, where k_0 is the wavenumber of the large amplitude pump wave, and ω and k denote the frequency and wave number of the perturbations. In the Hall current plasma case, the Alfvén-like waves consist of the whistler and ion cyclotron wave branches, which coalesce in the low-frequency MHD limit. Inhester (1990) considers kinetic models of these instabilities.

The standard perturbation analyses by the above authors consisted of obtaining coupled sound and Alfvén-like wave equations, with forcing terms due to the interaction of the pump wave with the perturbations, which involved sideband waves with frequencies and wavenumbers at $\omega_\pm = \omega \pm \omega_0$ and $k_\pm = k \pm k_0$. It was speculated by Goldstein (1978) that these instabilities were related to three-wave resonant interactions between two Alfvén waves and a slow magnetoacoustic wave in a low-beta plasma (e.g. Sagdeev and Galeev 1969). Jayanti and Hollweg (1993b) obtained a maximum growth rate for small plasma beta $0 < \beta < 1$, and for small pump wave amplitude δ, that corresponds (to within a numerical constant) to that obtained by Sagdeev and Galeev (1969), due to three-wave resonant interaction of the forward sound wave, the forward pump Alfvén wave and a backward, sideband Alfvén wave (the analysis assumes that β cannot be too close to zero or one). A different growth rate was obtained if both $\beta \to 0$ and $\delta \to 0$ simultaneously.

An alternative viewpoint of these instabilities is presented in this paper by using the wave mixing (or wave coupling) formalism for the interaction of linear waves in a non-uniform background flow developed by Webb et al. (1997,1999). In this development the large-amplitude pump Alfvén wave is regarded as the non-uniform background flow. Small-amplitude waves propagating in this background flow interact with each other due to gradients and time variations of the large-amplitude pump Alfvén wave (this process is somewhat analogous to the reflection and transmission of waves on a non-uniform string).

Section 2 presents a synopsis of the properties of simple Alfvén waves in one Cartesian space dimension. Section 3 discusses the general form of the wave mixing equations and the form of the wave interaction coefficients. Section 4 presents the form of the wave mixing equations for the special case where the background flow consists of a large-amplitude Alfvén wave, and compares this approach with the sideband Alfvén wave approach used by Goldstein (1978) and Derby (1978). Section 5 considers the solution of the initial value problem for the wave mixing equations for the special case where the pump Alfvén wave has a constant wavenumber $\mathbf{k}_0$ directed along the x axis. In this case, the wave interaction coefficients $\{\Lambda_{js}\}$ and the wave speeds $\{\lambda_j\}$ are all constants, and the wave mixing equations admit plane wave solutions in which the wave amplitudes $a_j \propto \exp[i(kx - \omega t)]$ (the index j labels the MHD wave modes). In this case, the dispersion equation $D(k, \omega) = 0$ obtained from the wave mixing equation formulation reduces to that obtained by Goldstein

https://doi.org/10.1017/S0022377801001283 Published online by Cambridge University Press

(1978) and Derby (1978). The general solution of the initial value problem in which the seven MHD wave mode amplitudes $\{a_j : 1 \leqslant j \leqslant 7\}$ are specified at time $t = 0$ is obtained by Fourier analysis. It is shown that the backward Alfvén wave $a_2(x, t)$ plays a special role as an intermediary via which the other waves interact with each other. The Green function solution (as defined by Bers 1983) is shown to play a pivotal role. We also discuss the results of Jayanti and Hollweg (1993b) on three-wave resonant interactions in the small-amplitude pump wave limit. In the short-wavelength limit ($k \to \infty$), the individual MHD wave modes decouple from each other, whereas at other wavelengths, the waves interact with each other due to gradients and time dependence of the background flow. In Sec. 6, we investigate solutions of the dispersion equation $D(k, \omega) = 0$. The regions of instability and the neutral stability surfaces, which depend parametrically on the properties of the large-amplitude Alfvén wave, are determined. Instabilities that arise from solving the dispersion equation $D(k, \omega) = 0$ both in the form $\omega = \omega^{(\alpha)}(k)$ (the index α labels the wave modes: $1 \leqslant \alpha \leqslant 5$), where k is real, and also solutions of the form $k = k^{(\alpha)}(\omega)$, where ω is real, are investigated. In Sec. 7, we look at the wave mixing equations from the perspective of a single master wave equation, with multiple modes, and with a source term due to the entropy wave. This is similar to the approach used by Whitham (1959,1974) in his discussion of wave hierarchies for short- and long-wavelength waves, and related work by Wu (1961). These methods are used to discuss wave stability. By expanding the dispersion equations for the different eigenmodes about $k = 0$, one obtains either the linearized Korteweg-deVries (KdV) or the Schrödinger equation as the generic wave equation at long-wavelengths, in which the wave dispersion coefficients depend on the amplitude of the pump wave. The corresponding short-wavelength ($k \to \infty$) dispersive wave equations are also obtained. Section 8 looks at initial value problems for the wave mixing equations. Two initial value problems are investigated. In the first problem, the equations are solved in closed form for the case of spatially periodic initial data. A second example studies the solution for hump or pulse-like initial data for one of the wave modes. The work of Briggs (1964), Bers (1983) and Brevdo (1988) on convective and absolute instabilities is used to show that an absolute instability develops. Fourier solutions and asymptotic analysis are used to study the instability. Section 9 concludes with a summary and discussion.

2. Alfvén simple waves

The ideal MHD equations consist of the mass continuity equation, the MHD momentum equation including the $\mathbf{J} \times \mathbf{B}$ force on the plasma ($\mathbf{J}$ is the electric current density and $\mathbf{B}$ is the magnetic induction), Faraday's law relating the time derivative of $\mathbf{B}$ to the curl of the electric field $\mathbf{E}$ (in the MHD limit, $\mathbf{E} = -\mathbf{u} \times \mathbf{B}$, where $\mathbf{u}$ is the fluid velocity), Gauss's law $\boldsymbol{\nabla} \cdot \mathbf{B} = 0$, the entropy advection equation, and an equation of state $p = p(\rho, S)$ relating the gas pressure p to the density ρ and the entropy S.

The distinguishing feature of simple waves in hyperbolic or near-hyperbolic systems of equations is that all the physical variables should depend only on a single phase function $\varphi(x, y, z, t)$, where $\varphi = \text{const}$ defines the wavefront (e.g. Boillat 1970). MHD simple waves in one Cartesian space dimension have been discussed in standard texts (e.g. Cabannes 1970; Akhiezer et al. 1975). It is also possible to obtain multidimensional simple waves in MHD (e.g. Webb et al. 1996) and in gas dynamics

https://doi.org/10.1017/S0022377801001283 Published online by Cambridge University Press

(Webb et al. 1998), but these more complicated simple waves will not be considered here. For MHD simple waves, the physical variables ρ, $\mathbf{u}$, $\mathbf{B}$, entropy S and gas pressure p all depend on a single phase function φ.

The forward-propagating, simple Alfvén wave in one Cartesian space dimension x has seven simple wave integrals (Cabannes 1970):

$$\mathbf{u} + \mathbf{b} = \mathbf{c}_1, \tag{2.1}$$

$$\rho = \rho_0, \qquad B_x = B_{x0}, \qquad S = S_0, \qquad B^2 = B_0^2, \tag{2.2}$$

where $\mathbf{c}_1$, ρ_0, S_0, B_{x0} and B_0 are constants, and

$$\mathbf{b} = \frac{\mathbf{B}}{(\mu\rho)^{1/2}}, \qquad b_x = \frac{B_x}{(\mu\rho)^{1/2}}, \tag{2.3}$$

define the Alfvén velocity $\mathbf{b}$ and Alfvén speed component b_x along the x axis. From the fact that both B_x and ρ are constant in the Alfvén simple wave, it follows that

$$b_x = \frac{B_{x0}}{(\mu\rho_0)^{1/2}}, \qquad u_x = u_{x0}, \qquad B_y^2 + B_z^2 = B_{\perp 0}^2, \tag{2.4}$$

are all constant in the one-dimensional simple Alfvén wave. All the physical variables in the wave depend on the dimensionless phase variable

$$\varphi = \frac{x - \lambda_6 t}{L} = \bar{x} - \bar{\lambda}_6 \bar{t}, \tag{2.5}$$

where $\lambda_6 = u_x + b_x$ is the characteristic speed of the wave along the x axis, L is a characteristic length scale for the wave, and $k_0 = 1/L$ is a characteristic wavenumber. From (2.4), $B_y^2 + B_z^2 = \text{const}$, so that the transverse magnetic field in the wave can be written in the form

$$\mathbf{B}_\perp = B_{\perp 0}(0, \cos\zeta, \sin\zeta)^T, \tag{2.6}$$

where $\zeta = \zeta(\varphi)$ is an arbitrary function of the wave phase φ. Similarly, from (2.1), the transverse fluid velocity $\mathbf{u}_\perp = (0, u_y, u_z)^T$ in the wave can be written in the form

$$\mathbf{u}_\perp = \mathbf{u}_{\perp 0} + \mathbf{b}_{\perp 0} - \frac{\mathbf{B}_\perp(\varphi)}{(\mu\rho)^{1/2}}, \tag{2.7}$$

where the subscript $\perp$ denotes components perpendicular to the propagation direction (the positive x-axis).

3. Wave mixing equations

From Webb et al. (1999), the interaction of linear MHD waves in a non-uniform background flow in one Cartesian space dimension x satisfy wave mixing equations of the form

$$\frac{\partial a_j}{\partial t} + \frac{\partial}{\partial x}(\lambda_j a_j) + \sum_{s=1}^{7} \Lambda_{js} a_s = 0, \qquad 1 \leqslant j \leqslant 7. \tag{3.1}$$

In (3.1), the $\{a_j : 1 \leqslant j \leqslant 7\}$ are the wave amplitudes for the MHD wave modes, and the $\{\lambda_j : 1 \leqslant j \leqslant 7\}$ are the corresponding wave phase velocities for the backward and forward fast magnetoacoustic waves (λ_1 and λ_7), the slow magnetoacoustic waves (λ_3 and λ_5), the Alfvén waves (λ_2 and λ_6), and the entropy wave (λ_4), where

https://doi.org/10.1017/S0022377801001283 Published online by Cambridge University Press

the wave speeds are ordered so that $\lambda_{j+1} > \lambda_j$. In particular,

$$\left.\begin{aligned} &\lambda_1 = u_x - c_f, \qquad \lambda_2 = u_x - b_x, \qquad \lambda_3 = u_x - c_s, \qquad \lambda_4 = u_x, \\ &\lambda_5 = u_x + c_s, \qquad \lambda_6 = u_x + b_x, \qquad \lambda_7 = u_x + c_f, \end{aligned}\right\} \tag{3.2}$$

where $b_x = B_x/(\mu\rho)^{1/2}$ is the Alfvén phase speed, and c_f and c_s are the fast and slow magnetoacoustic phase speeds respectively. The eigenvalue $\lambda_4 = u_x$ corresponds to the entropy wave. The wave amplitudes $\{a_j\}$ can be expressed in terms of the total MHD fluid perturbations $(\rho, \delta\mathbf{u}^T, \delta\mathbf{B}^T, \delta S)^T$. The 49 wave mixing coefficients $\{\Lambda_{js}\}$ in (3.1) are given by the formulae

$$\Lambda_{js} = \mathbf{L}_j \cdot \left(\frac{\partial}{\partial t} + \lambda_s \frac{\partial}{\partial x}\right) \mathbf{R}_s, \qquad 1 \leqslant j \leqslant 7, \qquad 1 \leqslant s \leqslant 7, \tag{3.3}$$

where the $\{\mathbf{L}_j\}$ and the $\{\mathbf{R}_s\}$ denote the left and right MHD eigenvectors for the case where the conserved densities $\tilde{\Psi} = (\rho, \rho\mathbf{u}^T, B_y, B_z, \rho S)^T$ are the basic physical variables used in the perturbation analysis.

If $\mathbf{B}_\perp = (0, B_y, B_z)^T \neq 0$, the wave amplitudes $\{a_1, a_3, a_4, a_5, a_7\}$ for the magnetoacoustic and entropy waves are related to the wave density perturbations $\{\rho_1, \rho_3, \rho_4, \rho_5, \rho_7\}$ by the equations

$$\rho_1 = \alpha_f a_1, \qquad \rho_3 = \alpha_s a_3, \qquad \rho_4 = a_4, \qquad \rho_5 = \alpha_s a_5, \qquad \rho_7 = \alpha_f a_7, \tag{3.4}$$

where

$$\alpha_f = \left(\frac{a^2 - c_s^2}{c_f^2 - c_s^2}\right)^{1/2}, \qquad \alpha_s = \left(\frac{c_f^2 - a^2}{c_f^2 - c_s^2}\right)^{1/2}, \tag{3.5}$$

$a = (\gamma p/\rho)^{1/2}$ is the gas sound speed and γ is the adiabatic index of the gas.

The Alfvén wave amplitudes a_2 and a_6 are related to the Alfvén wave magnetic field perturbations $\mathbf{B}_2$ and $\mathbf{B}_6$ by the equations

$$\mathbf{B}_j = (0, \beta_z, -\beta_y)^T a_j, \qquad j = 2, 6, \tag{3.6}$$

where $\beta_\perp = \mathbf{B}_\perp/B_\perp$ and $\mathbf{B}_\perp = (0, B_y, B_z)^T$. In the degenerate eigenvalue case in which $B_\perp \to 0$ and $a > b_x$, the wave amplitudes of the slow-mode waves are related to the magnetic field perturbations by $\mathbf{B}_j = -a(\mu^{1/2}/\rho^{1/2})\beta_\perp a_j$, $j = 3, 5$; but if $a < b_x$ then $\mathbf{B}_j = a(\mu^{1/2}/\rho^{1/2})\beta_\perp a_j$, $j = 1, 7$ for the fast-mode waves.

The wave interaction equations (3.1) and wave mixing coefficients (3.3) were derived from the linearized MHD equations. Thus, there are relations between the wave mixing coefficients that must necessarily be satisfied, which are consistent with the linearized MHD conservation equations. Thus, for example, using the MHD eigenrelations, the linearized mass continuity equation can be written in the form

$$\frac{\partial}{\partial t}\left(\sum_{j \neq 2,6} \rho_j\right) + \frac{\partial}{\partial x}\left(\sum_{j \neq 2,6} \lambda_j \rho_j\right) = 0, \tag{3.7}$$

where the $\{\rho_j : j = 1, 3, 4, 5, 7\}$ are the density perturbations for the magnetoacoustic waves and the entropy wave. Similarly, the linearized, normal momentum equation for the system can be expressed in the form

$$\frac{\partial}{\partial t}\left(\sum_{j \neq 2,6} \lambda_j \rho_j\right) + \frac{\partial}{\partial x}\left(\sum_{j \neq 2,6} \lambda_j^2 \rho_j\right) = 0, \tag{3.8}$$

https://doi.org/10.1017/S0022377801001283 Published online by Cambridge University Press

and the linearized entropy conservation equation is

$$\frac{\partial}{\partial t}\left(\bar{S}\sum_{j\neq 2,6}\rho_j-\gamma\rho_4\right)+\frac{\partial}{\partial x}\left(\bar{S}\sum_{j\neq 2,6}\lambda_j\rho_j-\gamma u_x\rho_4\right)=0, \tag{3.9}$$

where $\bar{S}=S/C_v$ is a normalized form of the gas entropy. It is straightforward to write down analogous linearized versions of the remaining MHD equations. These linearized equations impose constraints on the wave mixing coefficients $\{\Lambda_{js}\}$. Thus, for example, the linearized mass continuity equation (3.7) implies that

$$\begin{aligned}&(\delta_{j1}+\delta_{j7})\left(\frac{\partial\alpha_f}{\partial t}+\lambda_j\frac{\partial\alpha_f}{\partial x}\right)+(\delta_{j3}+\delta_{j5})\left(\frac{\partial\alpha_s}{\partial t}+\lambda_j\frac{\partial\alpha_s}{\partial x}\right)\\&-\alpha_f(\Lambda_{1j}+\Lambda_{7j})-\alpha_s(\Lambda_{3j}+\Lambda_{5j})-\Lambda_{4j}=0,\end{aligned} \tag{3.10}$$

where $j=1,3,4,5,7$, and δ_{jk} is the Kronecker delta symbol. Similar constraints are implied by the other linearized MHD equations.

4. Wave interactions and Alfvén simple waves

In this section, we consider the form of the wave mixing equations (3.1) for the case where the background flow consists of a large-amplitude, forward-propagating, planar, simple Alfvén wave of the type described in Sec. 2. Section 4.1 considers the form of the wave mixing equations. The alternative formulation of the wave interactions involving sideband Alfvén waves used by Goldstein (1978) and Derby (1978) is described in Sec. 4.2.

4.1. Wave mixing equations

Consider the form of the wave mixing equations (3.1), for the case where the background flow is a large-amplitude, forward-propagating Alfvén wave. From Webb et al. (1999), the wave mixing coefficients $\{\Lambda_{2j},\Lambda_{j2},\Lambda_{6j},\Lambda_{j6}:\ 1\leqslant j\leqslant 7\}$, involving Alfvénic perturbations of the background flow are non-zero, since $\mathbf{B}\cdot\boldsymbol{\nabla}\times\mathbf{B}\neq 0$ and $\mathbf{B}\cdot\boldsymbol{\nabla}\times\mathbf{u}\neq 0$ for an Alfvén simple wave. For a large-amplitude Alfvén wave (Sec. 2) as the background flow, it can be shown that

$$\mathbf{B}\cdot\boldsymbol{\nabla}\times\mathbf{B}=-B_{\perp 0}^2\eta,\qquad \mathbf{B}\cdot\boldsymbol{\nabla}\times\mathbf{u}=\frac{B_{\perp 0}^2}{(\mu\rho_0)^{1/2}}\eta, \tag{4.1}$$

where

$$\eta=\frac{1}{L}\frac{\partial\zeta}{\partial\varphi}, \tag{4.2}$$

and $\zeta(\varphi)$ is an arbitrary, but pre-specified function of the wave phase φ (Sec. 2). For this background flow, all the wave speeds $\{\lambda_j:\ 1\leqslant j\leqslant 7\}$ are constants (i.e. u_x, c_f, c_s, b_x and the sound speed a are constants). Similarly, the parameters α_f and α_s in (3.5) are constants. The detailed forms of the wave mixing coefficients $\{\Lambda_{js}\}$ are given in Webb et al. (1999). The wave mixing equations (3.1) in the present case reduce to

$$\frac{\partial a_1}{\partial t}+\frac{\partial}{\partial x}(\lambda_1 a_1)+\Lambda_{12}a_2=0, \tag{4.3}$$

$$\frac{\partial a_3}{\partial t}+\frac{\partial}{\partial x}(\lambda_3 a_3)+\Lambda_{32}a_2=0, \tag{4.4}$$

https://doi.org/10.1017/S0022377801001283 Published online by Cambridge University Press

$$\frac{\partial a_4}{\partial t} + \frac{\partial}{\partial x}(\lambda_4 a_4) = 0, \tag{4.5}$$

$$\frac{\partial a_5}{\partial t} + \frac{\partial}{\partial x}(\lambda_5 a_5) + \Lambda_{52} a_2 = 0, \tag{4.6}$$

$$\frac{\partial a_7}{\partial t} + \frac{\partial}{\partial x}(\lambda_7 a_7) + \Lambda_{72} a_2 = 0 \tag{4.7}$$

for the magnetoacoustic and entropy waves, whereas the Alfvén wave equations are

$$\frac{\partial a_2}{\partial t} + \frac{\partial}{\partial x}(\lambda_2 a_2) + \sum_{j \neq 2,6} \Lambda_{2j} a_j = 0, \tag{4.8}$$

$$\frac{\partial a_6}{\partial t} + \frac{\partial}{\partial x}(\lambda_6 a_6) + \sum_{j \neq 2,6} \Lambda_{6j} a_j = 0. \tag{4.9}$$

Equations (4.3)–(4.7) show that the magnetoacoustic waves are coupled via the non-uniform background gradients to the backward-propagating, small-amplitude Alfvén wave a_2. The entropy wave (a_4) is advected with the background flow, and is unaffected by the other waves. On the other hand, the Alfvén waves (equations (4.8) and (4.9)) are coupled to the magnetoacoustic waves and the entropy wave. Note that there is no direct coupling of the Alfvén waves to each other, but there is an indirect coupling since the magnetoacoustic waves are coupled to the backward Alfvén wave.

The detailed form of the wave mixing coefficients $\{\Lambda_{js}\}$ in (4.3)–(4.9) are given below. The non-zero wave mixing coefficients for the magnetoacoustic waves in (4.3)–(4.7) are

$$\left.\begin{aligned}
\Lambda_{12} &= -\frac{\rho^{1/2}}{\mu^{1/2} a^2} \alpha_s (a + c_s) b_x \eta, \\
\Lambda_{32} &= \frac{\rho^{1/2}}{\mu^{1/2} a^2} \alpha_f (a + c_f) b_x \eta, \\
\Lambda_{52} &= \frac{\rho^{1/2}}{\mu^{1/2} a^2} \alpha_f (a - c_f) b_x \eta, \\
\Lambda_{72} &= -\frac{\rho^{1/2}}{\mu^{1/2} a^2} \alpha_s (a - c_s) b_x \eta,
\end{aligned}\right\} \tag{4.10}$$

where η is given by (4.2).

The Alfvén wave mixing coefficients $\{\Lambda_{2j}\}$ in (4.8) are given by

$$\left.\begin{aligned}
\Lambda_{21} &= \frac{\mu^{1/2} \alpha_s c_s (a + c_s)(c_f + b_x)}{2\rho^{1/2} a} \eta, \\
\Lambda_{23} &= -\frac{\mu^{1/2} \alpha_f c_f (c_f + a)(c_s + b_x)}{2\rho^{1/2} a} \eta, \\
\Lambda_{24} &= -\frac{b_x B_{\perp 0}}{2\rho} \eta, \\
\Lambda_{25} &= -\frac{\mu^{1/2} \alpha_f c_f (c_f - a)(b_x - c_s)}{2\rho^{1/2} a} \eta, \\
\Lambda_{27} &= \frac{\mu^{1/2} \alpha_s c_s (a - c_s)(c_f - b_x)}{2\rho^{1/2} a} \eta,
\end{aligned}\right\} \tag{4.11}$$

https://doi.org/10.1017/S0022377801001283 Published online by Cambridge University Press

where $\mathbf{b}_\perp = \mathbf{B}_\perp/(\mu\rho)^{1/2}$. Similarly, for the forward Alfvén wave equation (4.9), the wave mixing coefficients $\{\Lambda_{6j}\}$ are given by

$$\left.\begin{aligned}
\Lambda_{61} &= \frac{\mu^{1/2}\alpha_s(c_f+b_x)(a-c_s)(2a+c_s)}{2\rho^{1/2}a}\eta,\\
\Lambda_{63} &= \frac{\mu^{1/2}\alpha_f(c_s+b_x)(c_f-a)(c_f+2a)}{2\rho^{1/2}a}\eta,\\
\Lambda_{64} &= \frac{b_x B_{\perp 0}}{2\rho}\eta,\\
\Lambda_{65} &= \frac{\mu^{1/2}\alpha_f(b_x-c_s)(c_f+a)(c_f-2a)}{2\rho^{1/2}a}\eta,\\
\Lambda_{67} &= -\frac{\mu^{1/2}\alpha_s(c_f-b_x)(a+c_s)(2a-c_s)}{2\rho^{1/2}a}\eta.
\end{aligned}\right\} \tag{4.12}$$

In the derivation of the above expressions for the wave mixing coefficients, it is useful to note the identities

$$\alpha_f^2+\alpha_s^2 = 1, \qquad \alpha_f\alpha_s = \frac{ab_\perp}{c_f^2-c_s^2}. \tag{4.13}$$

Symmetries of the wave mixing coefficients are discussed in Webb et al. (1999).

4.2. Sideband Alfvén wave approach

In the perturbation analyses by Goldstein (1978) and Derby (1978) of the simple Alfvén wave with constant wavenumber $\mathbf{k}_0 = (k_0, 0, 0)^T$ and frequency ω_0, the perturbation equations consist of a second-order wave equation for sound waves:

$$\left(\frac{\partial^2}{\partial t^2} - a^2\frac{\partial^2}{\partial x^2}\right)\delta\rho = \frac{1}{2\mu}\frac{\partial^2}{\partial x^2}\left(B_+\delta B_- + B_-\delta B_+\right), \tag{4.14}$$

where

$$B_\pm = B_y \pm iB_z, \qquad \delta B_\pm = \delta B_y \pm iB_z, \tag{4.15}$$

describe the transverse magnetic field of the pump Alfvén wave ($B_\pm$) and the sideband Alfvén waves ($\delta B_\pm$). In the Fourier (ω, k)-space representation of (4.14), sound waves with frequency and wavenumber (ω, k) are generated by the interaction of the sideband Alfvén waves with frequency and wavenumbers $(\omega \pm \omega_0, k \pm k_0)$ with the pump Alfvén wave with frequency and wavenumber components $(\pm\omega_0, \pm k_0)$. The sideband Alfvén waves in turn satisfy the wave equation

$$\left(\frac{\partial^2}{\partial t^2} - b_x^2\frac{\partial^2}{\partial x^2}\right)\delta B_\pm = Q_\pm(B_\pm, \delta\rho, \delta u_x), \tag{4.16}$$

where

$$Q_\pm = -\frac{\partial}{\partial x}\left(b_x^2\frac{\delta\rho}{\rho}\frac{\partial B_\pm}{\partial x} + \delta u_x\frac{\partial B_\pm}{\partial t} + \frac{\partial}{\partial t}(B_\pm\delta u_x)\right). \tag{4.17}$$

The density and velocity perturbations $\delta\rho$ and δu_x satisfy the perturbed continuity equation

$$\frac{\partial\delta\rho}{\partial t} + u_x\frac{\partial\delta\rho}{\partial x} + \rho\frac{\partial\delta u_x}{\partial x} = 0. \tag{4.18}$$

https://doi.org/10.1017/S0022377801001283 Published online by Cambridge University Press

Equation (4.16) shows that the sideband Alfvén waves are generated by the interaction of the sound waves with frequency and wavenumber (ω, k) with the pump wave with frequencies and wavenumbers $(\pm\omega_0, \pm k_0)$.

In the above analysis, the wave perturbations are assumed to be isentropic, and hence there are no terms in the equations corresponding to the entropy wave. This is in contrast to the wave mixing equations formulation in Sec. 4.1, where the role of entropy waves is included in the analysis. The above formulation of the wave interactions in (4.14)–(4.18) can be interpreted as being due to resonant interactions. However, this interpretation is strictly only valid in the limit of a small-amplitude pump Alfvén wave. In this limit, and for the case of a low-beta plasma, the fast magnetoacoustic wave speed c_f is approximately equal to the Alfvén speed b_x, and the slow magnetoacoustic speed c_s is approximately equal to the sound speed a. Thus, for a small-amplitude pump wave, the waves involved in the interactions can be identified as Alfvén waves (or pseudo-Alfvén waves) and sound waves. On the other hand, if the pump wave has a large-amplitude, the waves involved in the interactions from the wave mixing equations perspective consist of magnetoacoustic, Alfvén and entropy waves. The dispersion equation for the waves obtained from the analysis of (4.14)–(4.18) (Goldstein 1978; Derby 1978) turns out to be the same as for the wave mixing equation formulation in Sec. 4.1. This is to be expected, since both sets of equations in the case of isentropic perturbations describe the same physics.

5. Wave mixing and the initial value problem

For the special Alfvén simple wave considered by Goldstein (1978) and Jayanti and Hollweg (1993b), the function $\zeta = \zeta(\varphi) = \varphi$ in (2.6). In this case, the wave vector $\mathbf{k}_0 = (\varphi_x, 0, 0)^T = (1, 0, 0)^T/L$ is a constant vector; the wave mixing coefficients $\{\Lambda_{js}\}$ in (4.10)–(4.12) and the wave speeds $\{\lambda_j : 1 \leqslant j \leqslant 7\}$ are all constants, and $\eta = 1/L$. Furthermore, the initial value problem for the wave mixing equations (4.3)–(4.9) can then be solved by transform methods.

5.1. The initial value problem

Introducing the Fourier–Laplace transform

$$\bar{a}_j(s,k) = \int_0^\infty dt \int_{-\infty}^\infty dx \exp(-st - ikx) a_j(x,t) \tag{5.1}$$

$(1 \leqslant j \leqslant 7)$, the wave mixing equations (4.3)–(4.9) reduce to algebraic equations in transform space:

$$(s + ik\lambda_j)\bar{a}_j + \Lambda_{j2}\bar{a}_2 = \hat{a}_j(k,0), \qquad j = 1,3,5,7, \tag{5.2}$$

$$(s + ik\lambda_4)\bar{a}_4 = \hat{a}_4(k,0), \tag{5.3}$$

$$(s + ik\lambda_2)\bar{a}_2 + \sum_{j \neq 2,6} \Lambda_{2j}\bar{a}_j = \hat{a}_2(k,0), \tag{5.4}$$

$$(s + ik\lambda_6)\bar{a}_6 + \sum_{j \neq 2,6} \Lambda_{6j}\bar{a}_j = \hat{a}_6(k,0), \tag{5.5}$$

https://doi.org/10.1017/S0022377801001283 Published online by Cambridge University Press

where the $\{\hat{a}_j\}$,

$$\hat{a}_j(k,0) = \int_{-\infty}^{\infty} dx \exp(-ikx) a_j(x,0), \qquad 1 \leqslant j \leqslant 7, \tag{5.6}$$

are the Fourier transforms of the initial data.

The algebraic equation system (5.2)–(5.5) can be written in the matrix form

$$\mathbf{A}\bar{\mathbf{a}}(s,k) = \hat{\mathbf{a}}(k,0), \tag{5.7}$$

where $\bar{\mathbf{a}}$ is the column vector with jth component $\bar{a}_j$. Similarly, the vector $\hat{\mathbf{a}}(k,0)$ has jth component $\hat{a}_j(k,0)$. The matrix $\mathbf{A}$ in (5.7) has the form

$$\begin{aligned} A_{\alpha\beta} = {} & (s + ik\lambda_\alpha)\delta_{\alpha\beta} + \Lambda_{\alpha\beta}\delta_{\beta 2}(1 - \delta_{\alpha 2} - \delta_{\alpha 4} - \delta_{\alpha 6}) \\ & + \Lambda_{\alpha\beta}(\delta_{\alpha 2} + \delta_{\alpha 6})(1 - \delta_{\beta 2} - \delta_{\beta 6}), \end{aligned} \tag{5.8}$$

where $1 \leqslant \alpha \leqslant 7$ and $1 \leqslant \beta \leqslant 7$ and $\delta_{\alpha\beta}$ is the Kronecker delta symbol. Equation (5.7) can be solved for $\bar{\mathbf{a}}(s,k)$ provided the determinant $\mathscr{D}(k,s) = \det(\mathbf{A})$ is non-zero. The determinant $\mathscr{D}(k,s)$ can be written in the form

$$\mathscr{D}(k,s) = (s + ik\lambda_4)(s + ik\lambda_6)\bar{D}(k,s), \tag{5.9}$$

where

$$\begin{aligned} \bar{D}(k,s) = {} & (s + ik\lambda_1)(s + ik\lambda_2)(s + ik\lambda_3)(s + ik\lambda_5)(s + ik\lambda_7) \\ & - \nu_1(s + ik\lambda_3)(s + ik\lambda_5)(s + ik\lambda_7) - \nu_3(s + ik\lambda_1)(s + ik\lambda_5)(s + ik\lambda_7) \\ & - \nu_5(s + ik\lambda_1)(s + ik\lambda_3)(s + ik\lambda_7) - \nu_7(s + ik\lambda_1)(s + ik\lambda_3)(s + ik\lambda_5). \end{aligned} \tag{5.10}$$

The coefficients

$$\nu_j = \Lambda_{2j}\Lambda_{j2}, \qquad j = 1, 3, 5, 7, \tag{5.11}$$

in (5.10) describe how the magnetoacoustic waves couple to the backward, small-amplitude Alfvén wave a_2. If $\det(\mathbf{A}) \neq 0$, then (5.7) can be solved to yield the solution for $\bar{\mathbf{a}}$ in the form:

$$\bar{\mathbf{a}}(s,k) = \mathbf{A}^{-1}\hat{\mathbf{a}}(k,0), \tag{5.12}$$

where $\mathbf{A}^{-1}$ is the inverse of the matrix $\mathbf{A}$.

Writing $s = -i\omega$ in (5.9) yields the dispersion function for the system in the form

$$\mathscr{D}(k,s) = \tilde{\mathscr{D}}(k,\omega) = -(\omega - k\lambda_4)(\omega - k\lambda_6)D(k,\omega), \tag{5.13}$$

where $D(k,\omega) \equiv \bar{D}(k,s)$ is given by

$$\begin{aligned} D(k,\omega) = -i\big[& (\omega - k\lambda_1)(\omega - k\lambda_2)(\omega - k\lambda_3)(\omega - k\lambda_5)(\omega - k\lambda_7) \\ & + \nu_1(\omega - k\lambda_3)(\omega - k\lambda_5)(\omega - k\lambda_7) + \nu_3(\omega - k\lambda_1)(\omega - k\lambda_5)(\omega - k\lambda_7) \\ & + \nu_5(\omega - k\lambda_1)(\omega - k\lambda_3)(\omega - k\lambda_7) + \nu_7(\omega - k\lambda_1)(\omega - k\lambda_3)(\omega - k\lambda_5)\big]. \end{aligned} \tag{5.14}$$

Solutions of the dispersion equation $D(k,\omega) = 0$ yield information on the parametric instabilities in the system, which were first investigated by Goldstein (1978) and Derby (1978). We note for later reference that if the wavenumber–frequency pair (k,ω) satisfies the dispersion equation $D(k,\omega) = 0$, then the pairs $(-k,-\omega)$, (k^*,ω^*) and $(-k^*,-\omega^*)$ (the superscript $*$ denotes complex conjugation) also satisfy the dispersion equation. Parametric instabilities and the dispersion equation $D(k,\omega) = 0$ are explored in further detail in the next section.

https://doi.org/10.1017/S0022377801001283 Published online by Cambridge University Press

It is of interest to note that at short-wavelengths ($k \gg k_0$), where $k_0 \equiv \eta$ is the wavenumber of the pump wave, the dispersion equation $\tilde{\mathscr{D}}(k,\omega) = 0$ has the usual MHD wave modes $\omega = k\lambda_j$ as solutions. In this WKB limit, the individual wave modes decouple from the background flow (i.e. from the pump wave), whereas in the long-wave limit ($k \ll k_0$), the waves couple to each other due to gradients in the background flow, via the wave interaction coefficients $\{\nu_j : j = 1,3,5,7\}$. This characteristic of MHD wave interactions in non-uniform background flows is well known (e.g. Heinemann and Olbert 1980; Zhou and Matthaeus 1990; Webb et al. 1999).

It is a straightforward but tedious process to determine the solution for $\bar{\mathbf{a}}(s,k)$ from (5.12) by determining the inverse matrix $\mathbf{A}^{-1}$ using Cramer's rule. However, it is simpler to first solve (5.2)–(5.5) for $\bar{a}_2(s,k)$ and $\bar{a}_4(s,k)$. The remaining wave amplitudes $\{\bar{a}_j : j \neq 2,4\}$ may then be solved in terms of the solution for $\bar{a}_2(s,k)$ and the initial data. The solution for $\bar{a}_2(s,k)$ is given by

$$\bar{a}_2(s,k) = \frac{(s+ik\lambda_1)(s+ik\lambda_3)(s+ik\lambda_5)(s+ik\lambda_7)}{\bar{D}(k,s)} \left(\hat{a}_2(k,0) - \sum_{j\neq 2,6} \frac{\Lambda_{2j}\hat{a}_j(k,0)}{s+ik\lambda_j} \right), \tag{5.15}$$

where $\bar{D}(k,s)$ is given by (5.10). The other wave amplitudes are given by

$$\bar{a}_j(s,k) = \frac{\hat{a}_j(k,0) - \Lambda_{j2}\bar{a}_2(s,k)}{s+ik\lambda_j}, \qquad j = 1,3,5,7, \tag{5.16}$$

$$\bar{a}_4(s,k) = \frac{\hat{a}_4(k,0)}{s+ik\lambda_4}, \tag{5.17}$$

$$\bar{a}_6(s,k) = \frac{1}{s+ik\lambda_6} \left(\hat{a}_6(k,0) - \sum_{j\neq 2,6} \frac{\Lambda_{6j}\hat{a}_j(k,0)}{s+ik\lambda_j} + \bar{a}_2(s,k) \sum_{j\neq 2,4,6} \frac{\Lambda_{6j}\Lambda_{j2}}{s+ik\lambda_j} \right). \tag{5.18}$$

The required solution for the wave amplitudes in (x,t) space may now be obtained by using the inverse Fourier–Laplace transform:

$$a_j(x,t) = \frac{1}{2\pi i} \int_{c-i\infty}^{c+i\infty} ds \int_{-\infty}^{\infty} \frac{dk}{2\pi} \exp(st+ikx)\bar{a}_j(s,k), \tag{5.19}$$

where the transforms $\{\bar{a}_j(s,k)\}$ are given by (5.15)–(5.18). Alternatively, setting $s = -i\omega$, the transform (5.19) can be written as a double Fourier transform with respect to ω and k. The constant c determining the integration path in the inverse Laplace transform in (5.19) is chosen so that the path is to the right of all singularities in the complex s plane.

From (5.16)–(5.19), one can obtain the solution for the wave amplitudes $\{a_j(x,t) : j \neq 2\}$ in terms of the solution for $a_2(x,t)$ and the initial data. In particular,

$$a_4(x,t) = a_4(x-\lambda_4 t, 0), \tag{5.20}$$

$$a_j(x,t) = a_j(x-\lambda_j t, 0) - \Lambda_{j2} \int_0^t du\, a_2(x-\lambda_j u, t-u), \qquad j = 1,3,5,7, \tag{5.21}$$

are the solutions for the entropy wave and the magnetoacoustic waves in terms of $a_2(x,t)$ and the initial data. Similarly, using the convolution theorem for Laplace

https://doi.org/10.1017/S0022377801001283 Published online by Cambridge University Press

transforms, we obtain

$$a_6(x,t) = a_6(x-\lambda_6 t,0) + \sum_{j\neq 2,6} \frac{\Lambda_{6j}}{\lambda_6-\lambda_j}\int_0^t du\,[\lambda_j a_j(x-\lambda_j u,0) - \lambda_6 a_j(x-\lambda_6 u,0)] + \sum_{j\neq 2,4,6}\frac{\Lambda_{6j}\Lambda_{j2}}{\lambda_6-\lambda_j}\int_0^t du\int_0^u du'\,[\lambda_6 a_2(x-\lambda_6 u', u-u') - \lambda_j a_2(x-\lambda_j u', u-u')], \tag{5.22}$$

as the solution for the forward Alfvén wave $a_6(x,t)$ in terms of $a_2(x,t)$ and the initial data.

By using new integration variables, the solution (5.22) can be rewritten in the more suggestive form

$$a_6(x,t) = a_6(x-\lambda_6 t,0) + \sum_{j\neq 2,6} \frac{\Lambda_{6j}}{\lambda_6-\lambda_j}\int_o^t dt'\,[\lambda_j a_j(x-\lambda_j t',0) - \lambda_6 a_j(x-\lambda_6 t',0)] + \sum_{j\neq 2,4,6}\frac{\Lambda_{6j}\Lambda_{j2}}{\lambda_6-\lambda_j}\int_0^t dt'\int_{x-\lambda_6(t-t')}^{x-\lambda_j(t-t')} dx'\,a_2(x',t'), \tag{5.23}$$

Equation (5.23) shows that the solution for $a_6(x,t)$ consists of the initial value term $a_6(x-\lambda_6 t,0)$, some further initial-value-like terms representing the generation of a_6 from the interaction of the magnetoacoustic waves with the background flow, and the double integral over a triangular region of the (x',t') plane, representing the generation of a_6, by a two-stage process in which $a_2(x',t')$ interacts with the background flow to generate magnetoacoustic waves, and the subsequent interaction of the magnetoacoustic waves with the background to generate the forward Alfvén mode a_6. The domain of influence in the double integral over x' and t' consists of the triangular region bounded by the x' axis and the two characteristics $x'=x-\lambda_6(t-t')$ and $x'=x-\lambda_j(t-t')$ for the forward Alfvén wave a_6 and the the jth magnetoacoustic eigenmode, and with apex at $(x',t')=(x,t)$. It is straightforward to verify that the solutions (5.20), (5.21) and (5.23) satisfy the wave mixing equations (4.3)–(4.7) and (4.9).

By inverting the transform (5.15), the solution for $a_2(x,t)$ can be written in the form

$$a_2(x,t) = \prod_{j=1,3,5,7}\left(\frac{\partial}{\partial t}+\lambda_j\frac{\partial}{\partial x}\right)\left(\int_{-\infty}^{\infty} G(x-y,t)a_2(y,0)dy\right) - \sum_{j=1,3,5,7}\Lambda_{2j}\prod_{p\neq j,2,4,6}\left(\frac{\partial}{\partial t}+\lambda_p\frac{\partial}{\partial x}\right)\int_{-\infty}^{\infty} G(x-y,t)a_j(y,0)dy - \Lambda_{24}\prod_{j=1,3,5,7}\left(\frac{\partial}{\partial t}+\lambda_j\frac{\partial}{\partial x}\right)\int_0^t dt'\int_{-\infty}^{\infty} dy\,G(x-y,t')a_4(y,0), \tag{5.24}$$

where

$$G(x,t) = \int_{c-i\infty}^{c+i\infty}\frac{ds}{2\pi i}\int_{-\infty}^{\infty}\frac{dk}{2\pi}\,\frac{\exp(st+ikx)}{\bar{D}(k,s)}, \tag{5.25}$$

is the Green function of the system. Alternatively, setting $s=-i\omega$ in (5.25), the

https://doi.org/10.1017/S0022377801001283 Published online by Cambridge University Press

Green function can be written in the Fourier transform form

$$G(x,t) = \int_L \frac{d\omega}{2\pi} \int_F \frac{dk}{2\pi} \frac{\exp[i(kx - \omega t)]}{D(k,\omega)}. \tag{5.26}$$

The above analysis shows that the stability of the system is in effect governed by the properties of the Green function $G(x,t)$. In (5.26) the contour F must lie in a strip of the complex k plane including the real k axis, where the integrand is analytic. The contour L can be chosen as a line parallel to the real ω axis of the form $\omega = \omega_r + iL$, where L is a constant, which is chosen so that there are no singularities of the integrand in $\mathrm{Im}(\omega) > L$ (this latter constraint is necessary since we require $G(x,t) = 0$ for $t < 0$). Bers (1983) reviews space–time instabilities in plasmas in terms of the Green function for the system. In particular, Bers describes Fourier methods to determine whether the instabilities of the system associated with complex roots of the dispersion equation $D(k,\omega) = 0$ are absolute or convective instabilities.

In the next section, we investigate the dispersion function $D(k,\omega)$ in order to describe the parametric instabilities of the large-amplitude Alfvén wave studied by Goldstein (1978) and Derby (1978).

6. The dispersion equation

In this section, we investigate the solutions of the dispersion equation (5.14), i.e. $D(k,\omega) = 0$. The dispersion equation is equivalent to that obtained by Derby (1978) and Goldstein (1978) in their studies of Alfvén wave parametric instabilities (Sec. 6.1). In Sec. 6.2, we investigate solutions of the dispersion equation of the form $\omega = \omega(k_r)$, where $k_r \equiv k$ is assumed to be real. This includes a determination of the neutral stability curves $\beta = \beta(\bar{k},\theta)$ (for a fixed θ), where $\beta = a^2/b^2$ is the effective plasma beta, θ defines the pump wave amplitude via the equation

$$\delta = \frac{B_\perp}{B_x} = \tan\theta, \tag{6.1}$$

and $\bar{k} = k/k_0$ is the normalized wavenumber of the waves. This class of instabilities only occur for short-wavelength waves with $k > k_0$, and are associated with the merging of the slow-mode roots of the dispersion equation. The dependence of the instability growth rate $\gamma = \mathrm{Im}(\omega)/\omega_0$ on the plasma beta and the pump wave amplitude is then explored. Section 6.3 carries out a similar investigation of the roots of the dispersion equation of the form $k = k(\omega_r)$, where $\omega_r \equiv \omega$ is restricted to be real. In this case, there are spatially unstable roots $k = k_r(\omega_r) + ik_i(\omega_r)$ of the dispersion equation that occur when $\omega > \omega_0$ and $|k| < k_0$. These long-wavelength, modulational instabilities are associated with the merging of the fast mode roots of the dispersion equation. The question of whether the instabilities are absolute or convective is addressed in Sec. 8 by using pinch point analysis of the dispersion equation (e.g. Bers 1983).

6.1. The Derby and Goldstein dispersion equations

The dispersion equation $D(k,\omega) = 0$ in (5.14) depends on the parameters $\nu_j = \Lambda_{j2}\Lambda_{2j}$, $j = 1,3,5,7$ describing the coupling of the magnetoacoustic waves with the backward Alfvén wave a_2. Using (4.10) and (4.11) the parameters $\{\nu_j : j = 1,3,5,7\}$

https://doi.org/10.1017/S0022377801001283 Published online by Cambridge University Press

can be written in the form

$$\left.\begin{aligned}\nu_1 &= -\eta^2\alpha_s^2\frac{b_xc_s(a+c_s)^2(c_f+b_x)}{2a^3},\\ \nu_3 &= -\eta^2\alpha_f^2\frac{b_xc_f(a+c_f)^2(c_s+b_x)}{2a^3},\\ \nu_5 &= \eta^2\alpha_f^2\frac{b_xc_f(c_f-a)^2(b_x-c_s)}{2a^3},\\ \nu_7 &= -\eta^2\alpha_s^2\frac{b_xc_s(a-c_s)^2(c_f-b_x)}{2a^3},\end{aligned}\right\} \tag{6.2}$$

where $\eta \equiv k_0 = 1/L$. Noting that $c_f > b_x > c_s > 0$, (6.2) implies

$$\nu_5 > 0 \qquad \text{and} \qquad \nu_j < 0, \qquad j = 1, 3, 7. \tag{6.3}$$

Without loss of generality, we set $u_x = 0$ in the simple wave background flow (this is equivalent to using the Doppler-shifted frequency $\omega' = \omega - ku_{x0}$ if $u_{x0} \neq 0$). Using the wave phase speed $V_p = \omega/k$, the dispersion equation (5.14) assumes the form

$$D_p(V_p) \equiv G(V_p) + \frac{1}{k^2}F(V_p) = 0, \tag{6.4}$$

where

$$\begin{aligned}F(V_p) = {}&\nu_1(V_p-\lambda_3)(V_p-\lambda_5)(V_p-\lambda_7) + \nu_3(V_p-\lambda_1)(V_p-\lambda_5)(V_p-\lambda_7)\\ &+\nu_5(V_p-\lambda_1)(V_p-\lambda_3)(V_p-\lambda_7) + \nu_7(V_p-\lambda_1)(V_p-\lambda_3)(V_p-\lambda_5),\end{aligned} \tag{6.5}$$

$$G(V_p) = (V_p-\lambda_1)(V_p-\lambda_2)(V_p-\lambda_3)(V_p-\lambda_5)(V_p-\lambda_7). \tag{6.6}$$

To obtain Derby's form of the dispersion equation, we introduce the normalized frequencies and wavenumber $\bar\omega$ and $\bar k$, and normalized phase speed, or Alfvén Mach number M:

$$\bar\omega = \frac{\omega}{\omega_0}, \qquad \bar k = \frac{k}{k_0}, \qquad M = \frac{\bar\omega}{\bar k}, \tag{6.7}$$

where ω_0 and k_0 are the frequency and wavenumber of the pump wave (note that $\omega_0 = k_0b_x$, and $M \equiv V_p/b_x$). Now we note that

$$F(V_p) \equiv -4b_x^5k_0^2\left[M^3 - M^2 - \left(\beta_x + \tfrac{3}{4}\delta^2\right)M + \beta_x + \tfrac{1}{4}\delta^2\right], \tag{6.8}$$

where

$$\beta_x = \frac{a^2}{b_x^2}, \qquad \delta^2 = \frac{B_\perp^2}{B_x^2}, \tag{6.9}$$

are parameters describing the pump Alfvén wave. Using (6.5)–(6.9) in (6.4), the dispersion equation (6.4) reduces to the form

$$\bar k^2 = -\frac{F(V_p)}{k_0^2G(V_p)} \equiv \frac{4[M^3 - M^2 - (\beta_x + \frac{3}{4}\delta^2)M + \beta_x + \frac{1}{4}\delta^2]}{(M+1)(M^2-\bar\lambda_7^2)(M^2-\bar\lambda_5^2)}, \tag{6.10}$$

where

$$\bar\lambda_5 = \frac{c_s}{b_x}, \qquad \bar\lambda_7 = \frac{c_f}{b_x}, \tag{6.11}$$

are the normalized fast and slow magnetosonic speeds respectively. The dispersion equation (6.10) is equivalent to that obtained by Derby (1978). Using (6.3), (6.5)

https://doi.org/10.1017/S0022377801001283 Published online by Cambridge University Press

and (6.8), we find that the numerator in (6.10) has three real roots $M = N_1$, N_2 and N_3, where

$$\bar{\lambda}_1 < N_1 < \bar{\lambda}_3, \qquad \bar{\lambda}_5 < N_2 < \bar{\lambda}_6, \qquad \bar{\lambda}_6 < N_3 < \bar{\lambda}_7, \tag{6.12}$$

where $\bar{\lambda}_6 = 1$ (see also Derby 1978).

The dispersion equation (6.10) can also be written in the form

$$(\bar{\omega}^2 - \bar{k}^2\beta_x)(\bar{\omega} - \bar{k})[(\bar{\omega} + \bar{k})^2 - 4] = \bar{k}^2\delta^2(\bar{\omega}^3 + \bar{k}\bar{\omega}^2 - 3\bar{\omega} + \bar{k}), \tag{6.13}$$

which is the form of the dispersion equation obtained by Goldstein (1978).

6.2. Dispersion equation roots for k real

Using the dispersion equation in the form (6.4), or Derby's form (6.10), it is straightforward to show that the dispersion equation has five real roots for $\bar{\omega}(\bar{k})$ or for M in the long-wavelength regime $0 < k < k_0$. From the signs of $D_p(V_p)$ in (6.4) at $\{V_p = \lambda_j : 1 \leqslant j \leqslant 7\}$ it follows that the dispersion equation has five real roots for $k > k_0(4 + b_\perp^2/a^2)^{1/2}$. It turns out that instabilities can arise in the intermediate wavenumber regime:

$$k_0 < k < k_0\left(4 + \frac{b_\perp^2}{a^2}\right)^{1/2}, \tag{6.14}$$

(note that (6.14) is a necessary, but not sufficient condition for wave instability). In the wavenumber regime (6.14), the dispersion equation has three real roots for V_p, located in the ranges $V_p < \lambda_1$, $\lambda_1 < V_p < \lambda_3$ and $V_p > \lambda_7$. Below, we determine the unstable, complex-conjugate roots of the dispersion equation for ω in the unstable wavenumber regime:

$$k_0 < k_L(\beta, \theta) < k < k_U(\beta, \theta) < k_0\left(4 + \frac{b_\perp^2}{a^2}\right)^{1/2}, \tag{6.15}$$

where

$$\beta = \frac{a^2}{b^2}, \qquad \delta^2 = \frac{B_\perp^2}{B_x^2} = \tan^2\theta. \tag{6.16}$$

The surfaces $k = k_L(\beta, \theta)$ and $k = k_U(\beta, \theta)$ determine the neutral stability surfaces in $(\bar{k}, \beta, \theta)$ space. Note that k_L and k_U depend parametrically on the plasma beta β and on the pump wave amplitude $\delta = \tan\theta$.

The dispersion equation (6.10) has the form

$$\bar{k}^2 = \frac{\mathscr{N}(M)}{\mathscr{D}(M)} = \frac{4(M - N_1)(M - N_2)(M - N_3)}{(M + 1)(M^2 - \bar{c}_f^2)(M^2 - \bar{c}_s^2)} \equiv \Phi(M), \tag{6.17}$$

where $\bar{c}_f = c_f/b_x$ and $\bar{c}_s/b_x$. A typical plot of $\bar{k}^2 = \Phi(M)$ as a function of M is displayed in Fig. 1 for the case $\beta = 0.1$ and $\theta = 60°$ (i.e. $\delta = 3^{1/2}$). The zeros of $\Phi(M)$, $M = N_1$, N_2 and N_3 occur where the curves cut the M axis. The vertical asymptotes (the dotted lines) occur at the zeros of the denominator (i.e. at $M = -\bar{c}_f$, -1, $-\bar{c}_s$, $\bar{c}_s$ and $\bar{c}_f$). For the parameters used in the figure, the zero N_1 is located in the range $-\bar{c}_f < N_1 < -1$ (for larger plasma betas, the zero N_1 can lie in the range $-1 < N_1 < -\bar{c}_s$). The dotted horizontal lines at $\bar{k} = 1$ and at $\bar{k} = (4+b_\perp^2/a^2)^{1/2}$ correspond to the upper and lower bounds in (6.14). There are five real roots of the dispersion equation for M (and hence for ω) in the wavenumber regimes $\bar{k} > (4+b_\perp^2/a^2)^{1/2}$ and $0 < \bar{k} < 1$. There are only three real roots for M in the wavenumber regime $\bar{k}_L < \bar{k} < \bar{k}_U$, where $\bar{k}_U$ corresponds to the minimum of $\bar{k}^2 = \Phi(M)$ in the range $-\bar{c}_s < M < \bar{c}_s$, and

https://doi.org/10.1017/S0022377801001283 Published online by Cambridge University Press

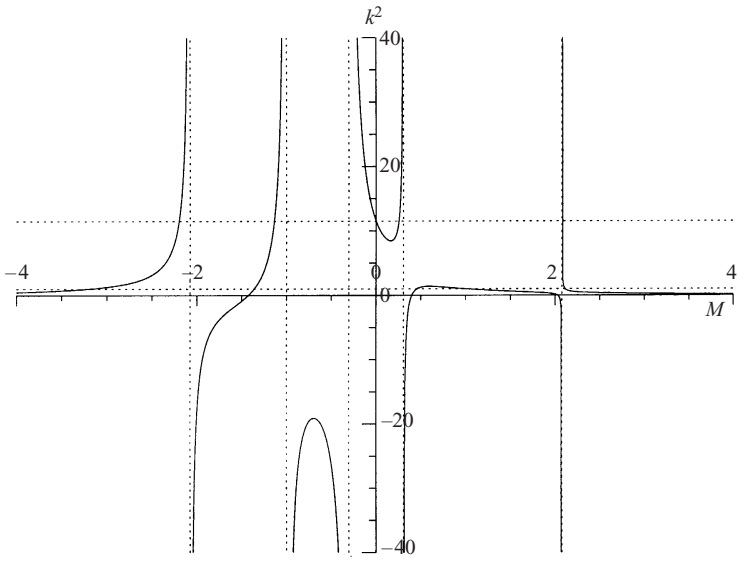


Figure 1. Plot of $\bar{k}^2$ versus M for the dispersion equation (6.17), where $M = \bar{\omega}/\bar{k}$ is the normalized phase speed. The parameters $\beta = 0.1$ and $\theta = 60°$. The dotted horizontal lines correspond to $\bar{k} = 1$ and $\bar{k} = (4 + b_\perp^2/a^2)^{1/2}$. Complex roots for M or $\bar{\omega}$ occur in the region where there are no real roots for $\bar{k}$ (i.e. in the region $1 < \bar{k}_L < \bar{k} < \bar{k}_U < (4 + b_\perp^2/a^2)^{1/2}$ and $M > 0$).

$\bar{k}_L$ corresponds to the maximum of $\Phi(M)$ in the range $\bar{c}_s < M < \bar{c}_f$. The Mach numbers $M = M_L$ and $M = M_U$ and corresponding neutral stability wavenumbers $\bar{k}_L(\beta, \theta)$ and $\bar{k}_U(\beta, \theta)$ can be determined by solving the equations $\Phi'(M) = 0$ and $\bar{k}^2 = \Phi(M)$ simultaneously for M and $\bar{k}$. These solutions correspond to the condition for the dispersion equation to have double real roots for M. For the parameters in Fig. 1, $M_L = 0.594\,19$ and $\bar{k}_L = 1.1768$; and $M_U = 0.163\,79$ and $\bar{k}_U = 2.9039$.

Figure 2 shows the neutral stability curves $\beta = \beta_L(\bar{k}, \theta)$ and $\beta = \beta_U(\bar{k}, \theta)$ corresponding to $\bar{k} = \bar{k}_L$ and $\bar{k} = \bar{k}_U$ for the case $\theta = 60°$. The dispersion equation has unstable roots for $\beta_L < \beta < \beta_U$ (i.e. for $\bar{k}_L < \bar{k} < \bar{k}_U$). Figure 3 shows how the instability regions in $(\bar{k}, \beta)$ space change with the amplitude of the pump wave $\delta = \tan\theta$ (in the figure, $\theta = 1°$, $10°$, $30°$ and $60°$). The region of instability in $(\bar{k}, \beta)$ parameter space shrinks as the pump wave amplitude $\delta = \tan\theta \to 0$ (i.e. as $\theta \to 0$).

For $\bar{k} \neq 2$, analysis of the dispersion equation (6.10) or (6.13) in the limit as $\delta = \tan\theta \to 0$ yields the form of the neutral stability curves $\beta_L(\bar{k}, \theta)$ and $\beta_U(\bar{k}, \theta)$ in the form

$$\beta_{U,L} = \left(\frac{2}{\bar{k}} - 1\right)^2 \pm 4\left(\frac{2}{\bar{k}} - 1\right) c_1\delta + O(\delta^2), \tag{6.18}$$

$$M_{L,U} = \frac{2}{\bar{k}} - 1 \pm c_1\delta + O(\delta^2), \tag{6.19}$$

where

$$c_1 = \left(\frac{\bar{k} - 1}{8(2 - \bar{k})}\right)^{1/2}, \tag{6.20}$$

and $1 < \bar{k} < 2$. To derive (6.19), it is probably simplest to rewrite the dispersion equation (6.13) in the form $M^2 - \beta_x = \delta^2 g(M, \bar{k})$ and then to note that the condition

https://doi.org/10.1017/S0022377801001283 Published online by Cambridge University Press

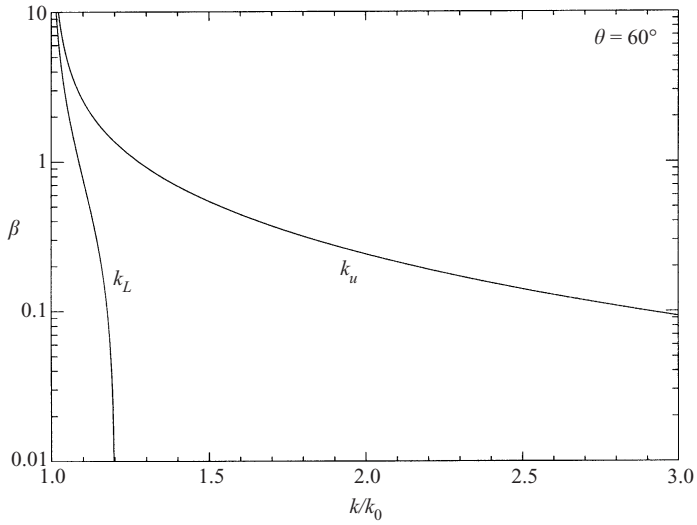


Figure 2. Neutral stability curves $\beta = \beta_L(\bar{k}, \theta)$ and $\beta = \beta_U(\bar{k}, \theta)$ or $\bar{k} = \bar{k}_L(\beta, \theta)$ and $\bar{k} = \bar{k}_U(\beta, \theta)$. The dispersion equation has complex roots for $\bar{\omega}$ or M in the region between the curves (i.e. for $\bar{k}_L < \bar{k} < \bar{k}_U$).

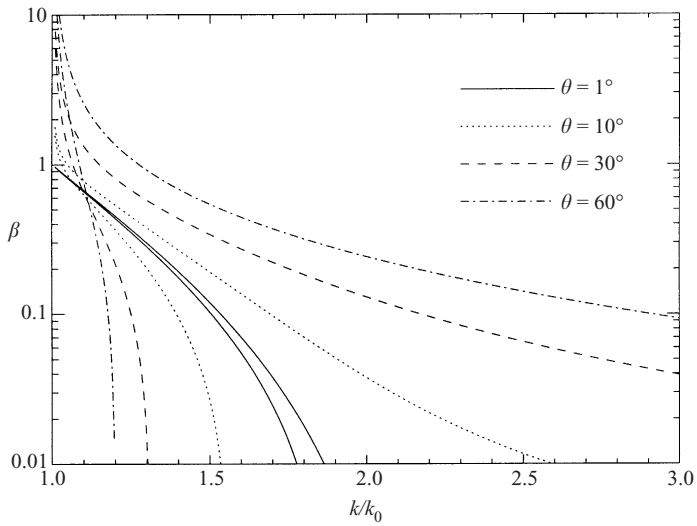


Figure 3. This plot shows how the instability regions in $(\bar{k}, \beta)$ space (the region between the curves) change as the pump wave amplitude $\delta = \tan\theta$ decreases ($\theta = 1°$, $10°$, $30°$ and $60°$).

for this equation to have a double root for M (i.e. the neutral stability condition) for a fixed $\bar{k}$ is $2M - \delta^2 \partial g/\partial M = 0$. The latter equation for small δ has solution of the form (6.19), and the first of these two equations then yields the required solution (6.18) for β.

Jayanti and Hollweg (1993b) obtained analytical growth rate approximations in the limit as the pump wave amplitude $\delta \to 0$. In particular, in the case where the pump wave amplitude $A = \delta^2 \equiv \tan^2\theta$ is small, and in the low-plasma-beta case ($0 < \beta < 1$), for which the plasma beta is not too small, they obtained the

https://doi.org/10.1017/S0022377801001283 Published online by Cambridge University Press

maximum growth rate of unstable waves as

$$\frac{\gamma_{\max}}{\omega_0} = N\frac{A^{1/2}(1-\beta^{1/2})^{1/2}}{\beta^{\frac{1}{4}}(1+\beta^{1/2})}, \qquad \text{where} \qquad N = \tfrac{1}{2}. \tag{6.21}$$

In their analysis, the zeroth-order solution of the dispersion equation is obtained by setting $\delta = 0$ in (6.13), to obtain the equation

$$(\bar{\omega}^2 - \bar{k}^2\beta_x)(\bar{\omega} - \bar{k})[(\bar{\omega} + \bar{k})^2 - 4] \simeq 0, \tag{6.22}$$

One can identify the roots of (6.22) in terms of three-wave resonant interactions. Thus, for example, the resonance conditions

$$\omega_- = \omega_0 - \omega, \qquad k_- = k_0 - k, \tag{6.23}$$

with dispersion equations

$$\omega_- = -k_- b_x, \qquad \omega = ka, \qquad \omega_0 = k_0 b_x, \tag{6.24}$$

represent the three-wave resonant interaction of the forward sound wave with frequency–wavenumber pair $(-\omega, -k)$ with the pump Alfvén wave (ω_0, k_0) to produce the backward, sideband Alfvén wave (ω_-, k_-). In terms of the normalized frequency and wavenumbers $\bar{\omega}$ and $\bar{k}$, the forward sound wave and the backward Alfvén wave have dispersion equations

$$\bar{\omega} - \bar{k}\beta_x^{1/2} = 0, \qquad \bar{\omega} + \bar{k} - 2 = 0, \tag{6.25}$$

which are readily recognized as two of the factors in the approximate dispersion equation (6.22). The simultaneous solution of (6.25) for $(\bar{\omega}, \bar{k})$ yield

$$\bar{\omega} = \frac{2\beta_x^{1/2}}{1+\beta_x^{1/2}} = \frac{2a}{a+b_x}, \qquad \bar{k} = \frac{2}{1+\beta_x^{1/2}} = \frac{2b_x}{a+b_x}, \tag{6.26}$$

as the lowest-order solution for $(\bar{\omega}, \bar{k})$. The growth rate of the unstable sound wave (6.21) can then be determined from a perturbation solution of (6.13) in which the wave amplitude A is a small parameter (Jayanti and Hollweg 1993b).

The growth rate (6.21) is the same, to within a numerical constant, as that given by Sagdeev and Galeev (1969) due to three-wave resonant interaction between the forward-propagating pump Alfvén wave with frequency ω_0, the forward-propagating sound wave with frequency ω, and the backward-propagating Alfvén wave with frequency $\omega_2 = \omega - \omega_0$. Sagdeev and Galeev (1969) obtained the same growth rate formula (6.21) for the sound wave, except that $N = N_{SG} = 2^{1/2}$. The instability growth rate in Sagdeev and Galeev (1969) is the growth rate of the envelopes of the backward Alfvén wave and the forward sound wave, which were assumed to be of much smaller amplitude than the pump Alfvén wave. The analysis of Sagdeev and Galeev (1969) assumed that there was exact resonance between the high frequency wave oscillations inside the wave envelopes. A similar analysis by Webb et al. (2000), also resulted in a growth rate for the unstable wave envelopes of the form (6.20), except that the normalization constant $N = N_w = 2^{-\frac{3}{2}}$. Related work on parametric wave interactions between acoustic and Alfvén waves in approximate resonance has been carried out by Hung (1974). Jayanti and Hollweg (1993b) noted that the growth rate (6.21) does not apply if both β and A are small and of the same order (i.e. if $\beta = \beta_0\epsilon$ and $A = A_0\epsilon$, where $0 < \epsilon \ll 1$). In the latter case, they obtained a finite maximum growth rate $\gamma_{\max}/\omega_0 \propto A^{1/3}$ as $\beta \to 0$ and as $A \to 0$.

https://doi.org/10.1017/S0022377801001283 Published online by Cambridge University Press

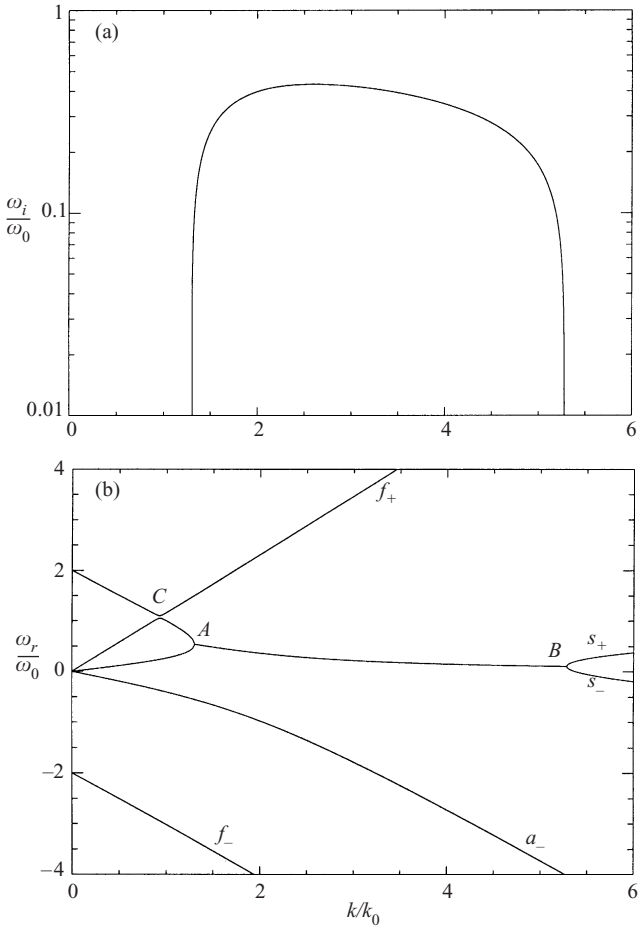


Figure 4. Instability growth rate ω_i/ω_0 (a) and real part of the frequency ω_r/ω_0 (b) versus k/k_0 for the case $\beta = 0.01$ and $\theta = 30°$.

Figure 4(a) shows the instability growth rate ω_i/ω_0 for the unstable mode as a function of $\bar{k}$, for the case $\beta = 0.01$ and $\theta = 30°$. Figure 4(b) shows the corresponding real parts of the roots ω_r/ω_0. The segment AB in the bottom panel corresponds to the unstable wavenumber regime $\bar{k}_L < \bar{k} < \bar{k}_U$ (i.e. $\bar{k} = \bar{k}_L$ at A, and $\bar{k} = \bar{k}_U$ at B). For $\bar{k} < \bar{k}_L$ and for $\bar{k} > \bar{k}_U$ the dispersion equation has five real roots. The points A and B are bifurcation points, where two real roots coalesce to form a complex-conjugate pair. At large wavenumbers (short wavelengths), the solutions of the dispersion equation for ω_r (Fig. 4b) are labelled as $f_\pm$ for the backward and forward fast-mode waves, $s_\pm$ for the backward and forward slow-mode waves, and a_- for the backward Alfvén wave. Near B, the backward and forward slow-mode branches coalesce, resulting in wave instability and complex-conjugate roots for the dispersion equation. The point C corresponds roughly to $(k, \omega) = (k_0, \omega_0)$, which is the wavenumber–frequency pair for the pump Alfvén wave. The phase speed of the different wave modes is given by ω/k, whereas the group velocity is given by the local slope $d\omega/dk$. It is also interesting to note that in the long-wavelength limit,

https://doi.org/10.1017/S0022377801001283 Published online by Cambridge University Press

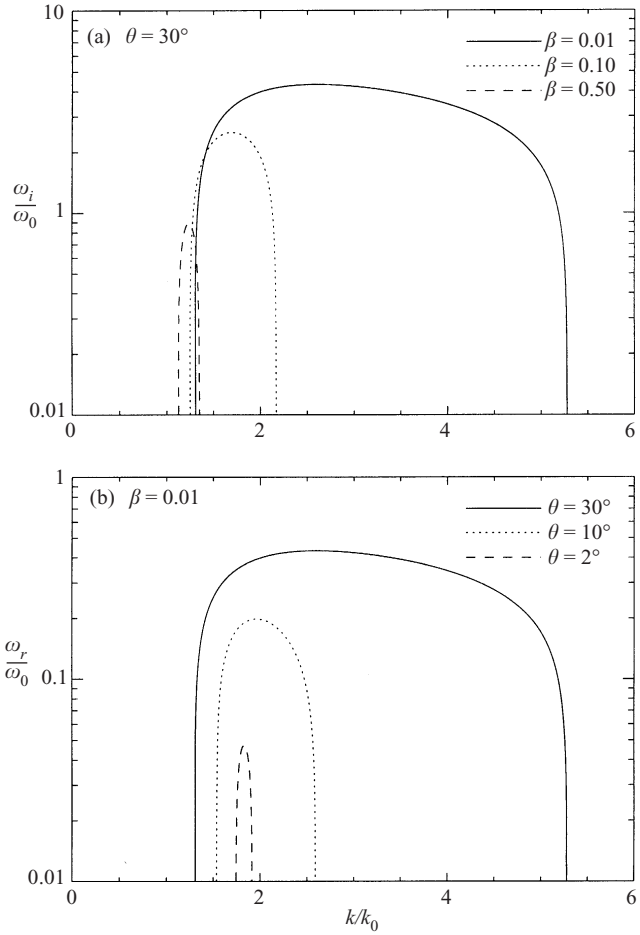


Figure 5. Instability growth rate ω_i/ω_0 versus k/k_0, and the parametric dependence of the instability on β and θ: (a) $\theta = 30°$ and $\beta = 0.01$, 0.1 and 0.5; (b) $\beta = 0.01$ and $\theta = 30°$, 10° and 2°.

$k \to 0$, the dispersion equation has five real roots, namely: $\omega = \pm 2\omega_0$ and three other roots with $\omega \simeq 0$.

Figure 5 shows the characteristic dependence of the growth rate ω_i/ω_0 on the plasma beta and on the parameter θ determining the pump wave amplitude $\delta = \tan\theta$. Figure 5(a), shows the dependence of ω_i on β ($\beta = 0.01$, 0.1 and 0.5) for $\theta = 30°$. The main points to note are the decrease in the growth rate with increasing β, and the decrease in the instability wavenumber range as β increases. The instability occurs at longer wavelengths as β increases. Figure 5(b) shows the decrease in the growth rate as the pump wave amplitude $\delta = \tan\theta$ decreases ($\theta = 30°$, 10° and 2° in the figure) for the case $\beta = 0.01$. The instability wavenumber range decreases as θ decreases. Further growth rate calculations and analytical approximations are given in Goldstein (1978), Derby (1978) and Jayanti and Hollweg (1993b).

6.3. Spatial instability

In order to classify the instability, it is useful to know if the dispersion equation (6.13) (i.e. $D(k, \omega) = 0$) has complex roots $\omega = \omega_r + i\omega_i$ for real k, or if it has complex

https://doi.org/10.1017/S0022377801001283 Published online by Cambridge University Press

roots for $k = k_r + ik_i$ for real ω (e.g. Swanson 1989). In the latter case, the wave is called an amplifying wave if the wave grows in the direction of the energy flow, and an evanescent wave if the wave decays in the direction of energy flow. A further distinction is whether the instability is an absolute or convective instability. If a finite source (in space and time) leads to growth at every point in space, then the instability is absolute. On the other hand, a convective instability propagates in space, and eventually decays in time at a fixed point in space as the disturbance moves past the observer. Sturrock (1958) concluded that a convective instability is of the same type as an amplifying wave.

To address these issues, it is useful to solve the dispersion equation (6.13) for $k = k(\omega)$ for real ω. Introducing the slowness vector

$$\chi = \frac{\bar{k}}{\bar{\omega}} \equiv \frac{1}{M}, \tag{6.27}$$

the dispersion equation (6.10) can be rewritten in the form

$$\bar{\omega}^2 = \frac{\hat{N}(\chi)}{\hat{D}(\chi)} \equiv \Psi(\chi), \tag{6.28}$$

where

$$\left.\begin{aligned} \hat{N}(\chi) = &\quad 4[(\beta_x + \tfrac{1}{4}\delta^2)\chi^3 - (\beta_x + \tfrac{3}{4}\delta^2)\chi^2 - \chi + 1], \\ \hat{D}(\chi) = &\quad (1 - \bar{c}_f^2\chi^2)(1 - \bar{c}_s^2\chi^2)(1 + \chi). \end{aligned}\right\} \tag{6.29}$$

It follows that from (6.10) et seq. $\hat{N}(\chi)$ has real roots n_1, n_2 and n_3 located in the ranges

$$-\frac{1}{\bar{c}_s} < n_1 < -\frac{1}{\bar{c}_f}, \qquad \frac{1}{\bar{c}_f} < n_2 < 1, \qquad 1 < n_3 < \frac{1}{\bar{c}_s}. \tag{6.30}$$

The dispersion equation (6.28) has five real roots for χ if $0 < \bar{\omega}^2 < 1$ or if $\bar{\omega}^2 > 4$. If $1 < \bar{\omega}^2 < 4$, the dispersion equation (6.28) for χ can have either (a) five real roots or (b) three real roots and a pair of complex-conjugate roots. In the latter case, one obtains spatially growing and decaying eigenmodes.

A typical plot of the right-hand side of (6.28) (i.e. of $\Psi(\chi)$ versus χ) for the parameter values $\beta = 0.1$ and $\theta = 60°$ is displayed in Fig. 6. The plot in Fig. 6 is similar to the alternative dispersion equation plot in Fig. 1. It is evident from Fig. 6 that there exists a range of frequencies $\bar{\omega}_L < \bar{\omega} < \bar{\omega}_U$ for which the dispersion equation admits complex solutions for χ and $\bar{k}$, where $\bar{\omega}_U$ corresponds to the positive minimum of $\bar{\omega}^2 = \Psi(\chi)$, and $\bar{\omega}_L$ corresponds to the positive maximum of $\Psi(\chi)$ in the figure. Note that $1 < \bar{\omega}_L^2 < \bar{\omega}_U^2 < 4$.

Figure 7 shows the neutral stability curves $\bar{\omega} = \bar{\omega}_L$ and $\bar{\omega} = \bar{\omega}_U$ in the $(\beta, \bar{\omega})$ plane for a range of wave amplitudes $\delta = \tan\theta$ ($\theta = 2°$, $10°$, $30°$ and $80°$). Note that the instability region $\bar{\omega}_L < \bar{\omega} < \bar{\omega}_U$ increases as the wave amplitude $\delta = \tan\theta$ increases. There is only a very narrow range of frequencies for which the instability occurs as $\theta \to 0$ (see e.g. the $\theta = 2°$ curve).

Figure 8(a) shows the dependence of the spatial growth rate k_i/k_0 on ω/ω_0 for the case $\beta = 0.1$ and $\theta = 60°$. Figure 8(b) shows the real parts of the roots k_r/k_0 as functions of ω/ω_0. The segment AB in (b) $\bar{\omega}_L < \bar{\omega} < \bar{\omega}_U$, corresponds to the region where there are unstable solutions of the dispersion equation for k. In (b) the curves are labelled as $f_\pm$ for the backward and forward fast-mode waves, $s_\pm$ for the slow-mode waves, and a_- for the backward Alfvén wave. This classification is based on

https://doi.org/10.1017/S0022377801001283 Published online by Cambridge University Press

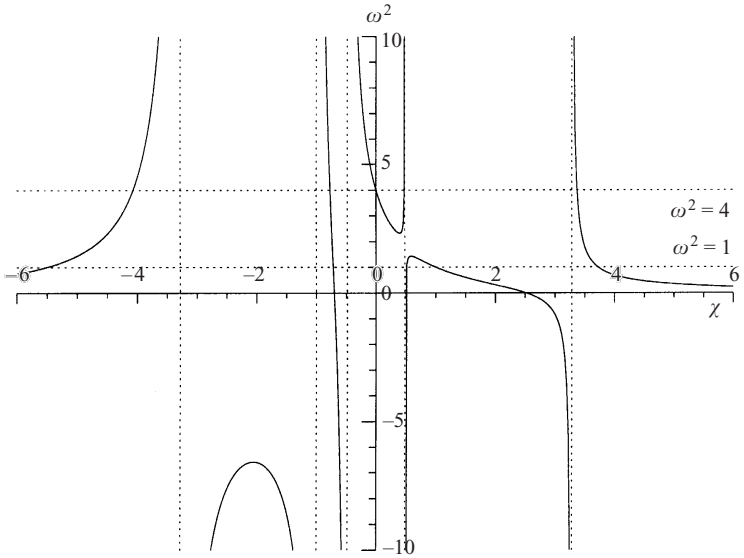


Figure 6. Plot of $\bar{\omega}^2$ versus χ for the dispersion equation (6.28), where $\chi = \bar{k}/\bar{\omega}$, for the case $\beta = 0.1$ and $\theta = 60°$. Unstable roots of the dispersion equation of the form $k = k_r(\omega) + ik_i(\omega)$ occur in the gap $1 < \bar{\omega}_L < \bar{\omega} < \bar{\omega}_U < 2$, where there are no curves.

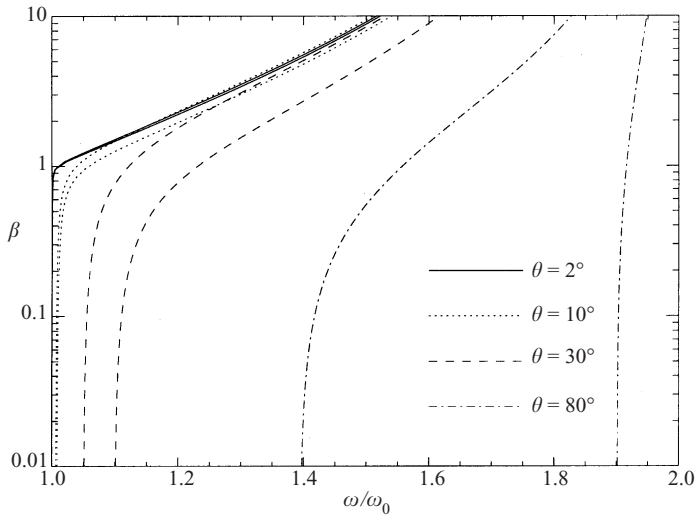


Figure 7. Neutral stability curves $\bar{\omega} = \bar{\omega}_L(\beta, \theta)$ and $\bar{\omega} = \bar{\omega}_U(\beta, \theta)$ in the $(\beta, \bar{\omega})$ plane for a range of θ ($\theta = 2°$, $10°$, $30°$ and $80°$). Unstable roots occur between the curves in the region $\bar{\omega}_L < \bar{\omega} < \bar{\omega}_U$.

the fact that at large wavenumbers and frequencies, the dispersion equation roots correspond to the usual MHD eigenmodes, and in this limit (i.e. the WKB limit), the different wave modes, to first order, propagate independently. The instability near B involves the coalescence of the backward and forward fast-mode waves. At the point A, $(\bar{\omega}_L, \bar{k}_L) = (1.2, 0.486)$; and at B, $(\bar{\omega}_U, \bar{k}_U) = (1.526, 0.259)$. Thus the unstable region AB occurs in the long-wavelength regime $0 < |\bar{k}| < 1$, i.e. the instability is a modulational instability (e.g. Hollweg 1994). This is in contrast to

https://doi.org/10.1017/S0022377801001283 Published online by Cambridge University Press

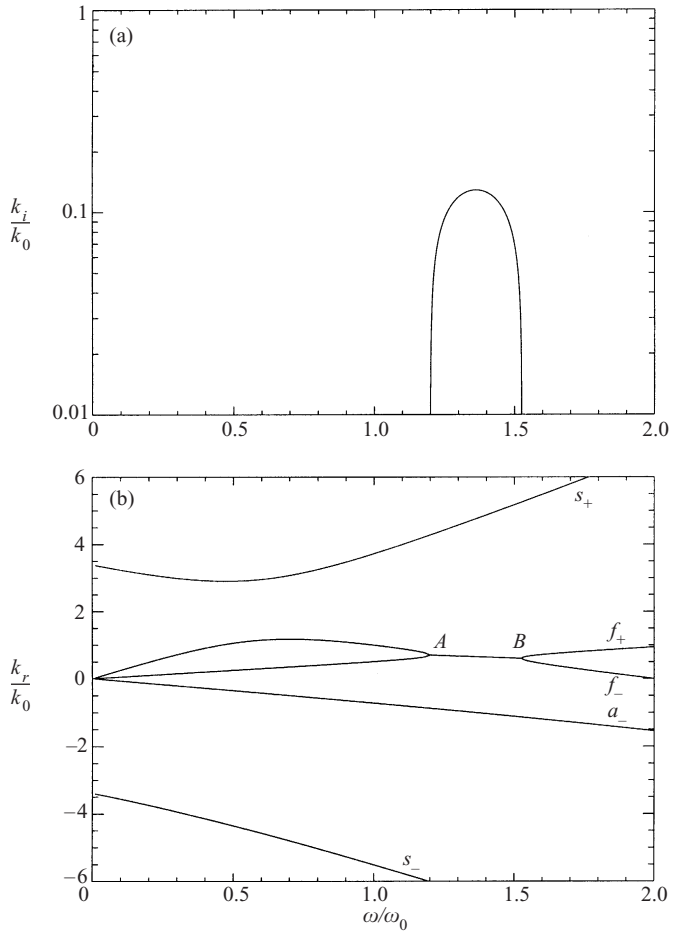


Figure 8. Spatial instability growth rate k_i/k_0 (a) and the real part of the wavenumber k_r/k_0 (b) versus ω/ω_0 for the case $\beta = 0.1$ and $\theta = 60°$.

the solutions for $\omega = \omega_r(k)+i\omega_i(k)$ in Fig. 4, where the instability occurs in the short-wavelength regime $|\bar{k}| > 1$, and the instability is of decay type (Hollweg 1994) and arises from the coalescence of the slow-mode branches of the dispersion equation. At low frequencies, ($\omega \to 0$), there are five real roots of the dispersion equation for k, namely the threefold root $k = 0$ and the roots $k = k_\pm = \pm k_0(4+b_\perp^2/a^2)^{1/2}$ (note that k_+ also occurs in the temporal stability case in (6.14) and (6.15)). The three roots with $k \simeq 0$ and $\omega \simeq 0$ correspond to solutions of the long-wavelength dispersion equation $N(\chi) = 0$ (see (6.29) et seq.), for which the normalized wave speeds or Alfvén Mach numbers have the numerical values $M_1 = -1.4253$, $M_2 = 0.398$ and $M_3 = 2.027$.

Figure 9 shows the dependence of the spatial growth rate k_i/k_0 on the plasma beta, and on the pump wave amplitude $\delta = \tan\theta$. Figure 9(a) shows the dependence of k_i on β ($\beta = 0.01$, 0.1, 1 and 10) for $\theta = 60°$. The growth rate k_i decreases as β increases, and the unstable band moves to higher frequencies ω. Figure 9(b) shows that the growth rate k_i/k_0 decreases as the pump wave amplitude $\delta = \tan\theta$

https://doi.org/10.1017/S0022377801001283 Published online by Cambridge University Press

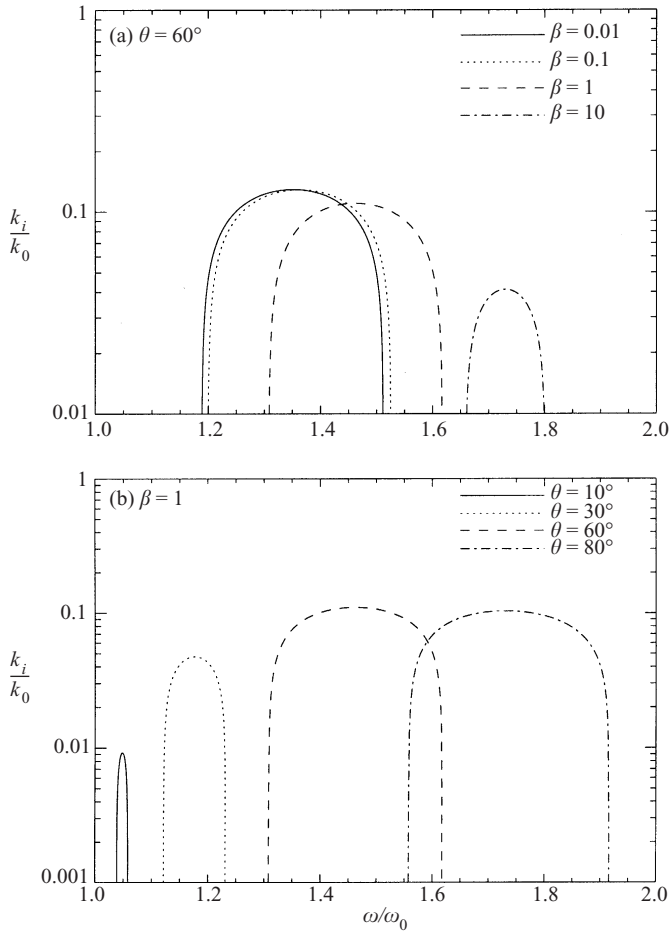


Figure 9. Spatial instability growth rate k_i/k_0 versus ω/ω_0, and the parametric dependence of the instability on β and θ: (a) $\theta = 60°$ and $\beta = 0.01$, 0.1, 1, and 10; (b) $\beta = 1$ and $\theta = 10°$, 30°, 60° and 80°.

decreases ($\theta = 10°$, 30°, 60° and 80°) for a $\beta = 1$ plasma. The unstable frequency range for ω increases in width and moves to higher frequency as θ increases.

7. Wave equations

In this section, we look at the wave mixing equations from the perspective of a single wave equation with multiple wave modes. This approach is similar to that adopted by Whitham (1959,1974) in his discussion of wave hierarchies and wave stability and related work by Wu (1961). As part of the analysis, we also investigate the character of the dispersion equation for long- and short-wavelength waves. By expanding the dispersion equation at long-wavelengths, one finds that the individual wave modes satisfy either the linearized Korteweg–deVries equation or the Schrödinger equation, in which the dispersion coefficients depend on the pump wave amplitude and the plasma beta. In Sec. 7.1, we obtain the wave equation for the system, in which the wave operator is directly related to the dispersion equation $D(k, \omega) = 0$. The results of Wu (1961) are used to establish the existence of an instability.

https://doi.org/10.1017/S0022377801001283 Published online by Cambridge University Press

Section 7.2 considers long-wavelength wave equations, and Sec. 7.3 derives short-wavelength wave equations.

7.1. Wave hierarchies and wave stability

From the wave mixing equations (4.3)–(4.9), it is straightforward to derive the master wave equation

$$\mathscr{L}[a_2] = -\Lambda_{24}\mathscr{F}[a_4], \tag{7.1}$$

governing the evolution of the backward Alfvén wave, $a_2(x,t)$, where the wave operator

$$\begin{aligned}\mathscr{L}(\partial_x,\partial_t) = {} & (\partial_t + c_1\partial_x)(\partial_t + c_2\partial_x)(\partial_t + c_3\partial_x)(\partial_t + c_4\partial_x)(\partial_t + c_5\partial_x) \\ & +4\omega_0^2(\partial_t + \Lambda_1\partial_x)(\partial_t + \Lambda_2\partial_x)(\partial_t + \Lambda_3\partial_x)\end{aligned} \tag{7.2}$$

is equivalent to $D(k,\omega)$ in (5.14) but with the replacements $k = -i\partial_x$ and $\omega = i\partial_t$ (i.e. $\mathscr{L}(\partial_x,\partial_t) = D(-i\partial_x, i\partial_t)$). In (7.2), the $\{c_j : 1 \leqslant j \leqslant 5\}$ are the short-wavelength speeds of the system, where $c_{j+1} > c_j$, i.e.

$$c_1 = \lambda_1, \qquad c_2 = \lambda_2, \qquad c_3 = \lambda_3, \qquad c_4 = \lambda_5, \qquad c_5 = \lambda_7, \tag{7.3}$$

and $a_4(x,t)$ in (7.1) is the entropy wave amplitude. At long-wavelengths ($k \to 0$) the dispersion equation $D(k,\omega) = 0$ has solutions to lowest order

$$\omega^{(1)} = -2\omega_0, \qquad \omega^{(2)} = k\Lambda_1, \qquad \omega^{(3)} = k\Lambda_2, \qquad \omega^{(4)} = k\Lambda_3, \qquad \omega^{(5)} = 2\omega_0. \tag{7.4}$$

The wave speeds $\{\Lambda_j : 1 \leqslant j \leqslant 3\}$ in (7.4) are related to the normalized wave speeds $\{N_j\}$ in (6.12) and (6.17) by the equations

$$\Lambda_j = b_x N_j, \qquad 1 \leqslant j \leqslant 3. \tag{7.5}$$

From (6.12), $\Lambda_1 < \Lambda_2 < \Lambda_3$ and

$$\lambda_1 < \Lambda_1 < \lambda_3, \qquad \lambda_5 < \Lambda_2 < \lambda_6, \qquad \lambda_6 < \Lambda_3 < \lambda_7. \tag{7.6}$$

The operator $\mathscr{F}(\partial_x,\partial_t)$ on the right-hand side of (7.1) is given by

$$\mathscr{F}(\partial_x,\partial_t) = (\partial_t + \lambda_1\partial_x)(\partial_t + \lambda_3\partial_x)(\partial_t + \lambda_5\partial_x)(\partial_t + \lambda_7\partial_x), \tag{7.7}$$

which is the short-wavelength magnetoacoustic operator for the system. Note that the long-wavelength phase speeds $V_p^{(1)} = -2\omega_0/k$ and $V_p^{(5)} = 2\omega_0/k$ in (7.4) diverge as $k \to 0$.

Equation (7.1) shows that the solutions for $a_2(x,t)$ consist of particular solutions, which are excited by the entropy wave perturbations present in the initial data, plus complementary solutions satisfying the homogeneous wave equation $\mathscr{L}[a_2] = 0$. These latter solutions are associated with magnetoacoustic and Alfvén wave perturbations in the initial data. As in Sec. 5, once the solution for $a_2(x,t)$ is found, the other wave amplitudes $\{a_j : j \neq 2\}$ can then be readily determined.

Wu (1961) studied the stability of wave equations of the form $\mathscr{L}(\partial_x,\partial_t)\psi = 0$, in which the number of short-wavelength waves n exceeds the number of finite phase speeds at long-wavelengths m by 2 (i.e. $n = m + 2$; in our case, $n = 5$ and $m = 3$). Wu (1961) and Whitham (1959, 1974) also studied the case $n = m + 1$. In the case, $n = m + 2$, Wu established that plane wave solutions of $\mathscr{L}\psi = 0$ of the form

$$\psi = \exp[ik(x - Ct)] \tag{7.8}$$

were stable if the c_j and Λ_j occur in neighbouring pairs and that instability can

https://doi.org/10.1017/S0022377801001283 Published online by Cambridge University Press

occur for some range of k otherwise (it is assumed $0 < k < \infty$). In our case, the wave speeds are ordered as

$$c_1 < c_2 < \Lambda_1 < c_3 < c_4 < \Lambda_2 < \Lambda_3 < c_5, \tag{7.9}$$

which implies that instability can occur for some range of k, since, for example, the long-wavelength speeds Λ_2 and Λ_3 are adjacent to each other in (7.9). Wu's stability criterion can be obtained by graphical means (although this is not explicitly stated in Wu's paper). Thus, in our case, $\mathscr{L}\psi = 0$ has plane wave solutions of the form (7.8) if

$$k^2 = \frac{4\omega_0^2(C-\Lambda_1)(C-\Lambda_2)(C-\Lambda_3)}{(C-c_1)(C-c_2)(C-c_3)(C-c_4)(C-c_5)}. \tag{7.10}$$

Equation (7.10) is equivalent to the dispersion equation form (6.17). The existence of an instability can be established by plotting k^2 versus C, which is in fact the method used in Fig. 1 (see also Derby 1978).

7.2. The long-wavelength limit

In the long-wavelength limit ($k \to 0$), the five solutions of the dispersion equation $\{\omega^{(\alpha)} : 1 \leqslant \alpha \leqslant 5\}$ are given to lowest order by (7.4). An improved description of these eigenmodes can be obtained by Taylor series expansion of the dispersion equation about $k = 0$ of the form

$$\omega^{(\alpha)} = \omega^{(\alpha)}(0) + \left(\frac{d\omega^{(\alpha)}}{dk}\right)_0 k + \frac{1}{2}\left(\frac{d^2\omega^{(\alpha)}}{dk^2}\right)_0 k^2 + \frac{1}{6}\left(\frac{d^3\omega^{(\alpha)}}{dk^3}\right)_0 k^3 + \ldots, \tag{7.11}$$

where the superscript α ($1 \leqslant \alpha \leqslant 5$) denotes the wave mode. The derivatives $(d^n\omega^{(\alpha)}/dk^n)_0$ in (7.11) can be obtained, for example, by implicit differentiation of the dispersion equation in the form (6.28), or otherwise.

In the case of the modes $\omega^{(j+1)} = k\Lambda_j$, $1 \leqslant j \leqslant 3$, a simpler, equivalent procedure of Whitham (1959,1974) can be used. Thus, for example, the mode $\omega^{(2)} = k\Lambda_1$ is equivalent at lowest order to the unidirectional wave equation

$$(\partial_t + \Lambda_1\partial_x)\psi \simeq 0. \tag{7.12}$$

An improved description of the wave may be obtained from the wave equation $\mathscr{L}\psi = 0$, by setting $\partial_t = -\Lambda_1\partial_x$ for all time derivatives in $\mathscr{L}$, except for the $\partial_t + \Lambda_1\partial_x$ term. Using these approximations, one obtains the approximate wave equation

$$\mathscr{L}\psi \simeq 4\omega_0^2(\Lambda_2-\Lambda_1)(\Lambda_3-\Lambda_1)\partial_x^2[\partial_t + \Lambda_1\partial_x + \gamma_1\partial_x^3]\psi = 0, \tag{7.13}$$

where

$$\gamma_1 = \frac{(\lambda_1-\Lambda_1)(\lambda_2-\Lambda_1)(\lambda_3-\Lambda_1)(\lambda_5-\Lambda_1)(\lambda_7-\Lambda_1)}{4\omega_0^2(\Lambda_2-\Lambda_1)(\Lambda_3-\Lambda_1)}. \tag{7.14}$$

Hence an improved description of the wave is given by the linearized Korteweg–deVries (KdV) equation

$$(\partial_t + \Lambda_1\partial_x + \gamma_1\partial_x^3)\psi = 0. \tag{7.15}$$

Using the identifications $\partial_t = -i\omega$ and $\partial_x = ik$ in (7.15) gives the KdV dispersion equation

$$\omega = k\Lambda_1 - \gamma_1 k^3. \tag{7.16}$$

The dispersion equation (7.16) could of course, also be obtained by Taylor series expansion (7.11), by implicit differentiation of the dispersion equation (6.28).

https://doi.org/10.1017/S0022377801001283 Published online by Cambridge University Press

By using the fact that the long-wavelength speeds $\{\Lambda_j : 1 \leqslant j \leqslant 3\}$ satisfy the cubic

$$\Lambda^3 - b_x\Lambda^2 - \left(a^2 + \tfrac{3}{4}b_\perp^2\right)\Lambda + \left(a^2 + \tfrac{1}{4}b_\perp^2\right)b_x = 0, \tag{7.17}$$

one can show that

$$\Lambda^4 - (a^2 + b^2)\Lambda^2 + a^2 b_x^2 = -\tfrac{1}{4}b_\perp^2(\Lambda - b_x)^2. \tag{7.18}$$

Using (7.18) in (7.14) then yields the alternative expression

$$\gamma_1 = \frac{b_\perp^2}{16\omega_0^2}\frac{(\Lambda_1 - b_x)^2(\Lambda_1 + b_x)}{(\Lambda_2 - \Lambda_1)(\Lambda_3 - \Lambda_1)} \tag{7.19}$$

for the dispersion coefficient γ_1. Equation (7.19) shows that $\gamma_1 \to 0$ as the pump wave amplitude $\delta = b_\perp/b_x \to 0$, which is intuitively expected, since the wave dispersion is due to the pump wave. Also from (7.19),

$$\mathrm{sgn}(\gamma_1) = \mathrm{sgn}(\Lambda_1 + b_x) \tag{7.20}$$

for the sign of γ_1. It is clear that the other long-wavelength wave modes of the form $\omega^{(j+1)} = k\Lambda_j$ with $j = 2, 3$, will also satisfy linearized KdV equations of the form (7.15), but with different coefficients. An inspection of the dispersion equation plot in Fig. 1 shows that the branch $\omega = k\Lambda_1$ near $k = 0$ becomes the backward Alfvén wave as $k \to \infty$. Similarly, the branches $\omega = k\Lambda_2$ and $\omega = k\Lambda_3$ near $k = 0$ can be associated with the backward and forward slow-mode solutions as $k \to \infty$.

The solutions with $\omega = \pm 2\omega_0$ as $k \to 0$ have phase speeds $V_p = \pm 2\omega_0/k$, which diverge as $k \to 0$, but their group velocity $V_G = (d\omega/dk)_0 = -b_x$ is finite. In Fig. 1, these two modes become the backward and forward fast-mode waves as $k \to \infty$. Differentiating the dispersion equation (6.28) implicitly with respect to k, for these modes yields the Taylor series coefficients

$$\omega(0) = \pm 2\omega_0, \qquad \left(\frac{d\omega}{dk}\right)_0 = -b_x, \qquad \left(\frac{d^2\omega}{dk^2}\right)_0 = \frac{\pm b_\perp^2}{8\omega_0} \tag{7.21}$$

at $k = 0$. Using the association $\omega = i\partial_t$ and $k = -i\partial_x$ and the Taylor series coefficients (7.21) in (7.11) yields the Schrödinger equation

$$\left(i(\partial_t - b_x\partial_x) \pm \frac{b_\perp^2}{16\omega_0}\partial_x^2 \mp 2\omega_0\right)\psi = 0 \tag{7.22}$$

as the improved long-wavelength wave equation governing the $\omega = \pm 2\omega_0$ modes. Again it is interesting to note that the coefficient of the dispersive term involving ∂_x^2 vanishes as the pump wave amplitude $\delta = b_\perp/b_x \to 0$. The term $V = \pm 2\omega_0$ in (7.22) is analogous to the potential in Schrödinger's equation.

The weakly nonlinear generalization of the linearized KdV equation (7.15) could be either the modified KdV equation or the KdV equation. Since the long-wavelength Schrödinger equation most likely describes wave modulation, we expect that the nonlinear generalization of the Schrödinger equation (7.22) would be the nonlinear Schrödinger equation. It is worth noting that the dispersion term in the above long-wavelength wave equations (7.15) and (7.22) is due to the interaction of the small-amplitude waves with the large-amplitude pump. This is a distinctly different process than that usually invoked to obtain wave dispersion in MHD plasmas, namely Hall current dispersion.

https://doi.org/10.1017/S0022377801001283 Published online by Cambridge University Press

7.3. Short-wavelength limit

As a typical example of an evolution equation for the short-wavelength waves, consider the mode with $\omega = k\lambda_1$ (the backward fast magnetoacoustic eigenmode) for large k, for which the lowest-order wave equation is

$$(\partial_t + \lambda_1\partial_x)\psi \simeq 0. \tag{7.23}$$

Setting $\partial_t = -\lambda_1\partial_x$ in all terms in the wave operator $\mathscr{L}(\partial_x, \partial_t)$ in (7.2), except in the term $\partial_t + \lambda_1\partial_x$, yields the modified, short-wavelength equation

$$[\partial_x(\partial_t + \lambda_1\partial_x) + \Gamma_1]\psi = 0, \tag{7.24}$$

where

$$\Gamma_1 = \frac{4\omega_0^2(\Lambda_1 - \lambda_1)(\Lambda_2 - \lambda_1)(\Lambda_3 - \lambda_1)}{(\lambda_2 - \lambda_1)(\lambda_3 - \lambda_1)(\lambda_5 - \lambda_1)(\lambda_7 - \lambda_1)}. \tag{7.25}$$

The modified dispersion equation corresponding to (7.24) is

$$\omega = k\lambda_1 - \frac{\Gamma_1}{k}. \tag{7.26}$$

Hence the wave phase speed $V_p = \omega/k = \lambda_1 - \Gamma_1/k$ is slightly modified for large k from $V_p = \lambda_1$. Similar results can be obtained for the other short-wavelength modes.

8. Initial value problems and wave stability

In this section, we present analytical and numerical solutions of the wave mixing equations (3.1). A variety of solutions can be obtained, depending on the initial data and the pump wave amplitude and the plasma beta. Analytical solutions of the wave mixing equations (4.3)–(4.9) for periodic initial data with a fixed wavenumber $k = K$ are presented in Sec. 8.1. In this case, closed form solutions can be obtained by Fourier–Laplace inversion. The detailed solution form depends on the solution of the dispersion equation $D(K, \omega) = 0$, in the form $\{\omega = \omega_\alpha(K) : \ 1 \leqslant \alpha \leqslant 5\}$. Depending on the value of K and the background plasma state, two of the dispersion equation roots can be complex conjugates for real K (see Sec. 6.2). Section 8.2 considers whether the instability is a convective or absolute instability (e.g. Briggs 1964; Bers 1983; Brevdo 1988) for the case in which the initial data is sharply peaked. In this case, it is important to investigate the behaviour of the dispersion equation for complex k and ω. The instability is illustrated using sample numerical solutions of the wave mixing equations.

8.1. Periodic solution example

Below, we give analytical solutions of the wave mixing equations (4.3)–(4.9) for the initial data

$$a_2(x, 0) = A_2\cos(Kx), \qquad a_j(x, 0) = 0, \qquad j = 1, 3, 4, 5, 6, 7, \tag{8.1}$$

where A_2 is a constant. This corresponds to specifying a single periodic wave mode at time $t = 0$ for the backward Alfvén wave $a_2(x, t) \neq 0$ at time $t = 0$. Similar solutions can be obtained by setting $a_{j_1} = a_{j_1}(x, 0) \neq 0$ at time $t = 0$, and $a_j(x, 0) = 0$ for $j \neq j_1$. It is evident from (4.3)–(4.9) that the backward Alfvén wave $a_2(x, t)$ plays an important role in mediating the interaction between the different wave modes.

There are three different solution forms for the initial value problem (8.1), de-

https://doi.org/10.1017/S0022377801001283 Published online by Cambridge University Press

pending on the character of the roots of the dispersion equation $D(K,\omega)=0$, (5.14), which depend parametrically on the background state. These cases are:

(i) $D(K,\omega)=0$ has five simple real roots (the stable case);

(ii) $D(K,\omega)=0$ has three simple, real roots ω_1, ω_2 and ω_5, and a pair of complex conjugate roots $\omega_3=\omega_{3r}+i\omega_{3i}$ and $\omega_4=\omega_{3r}-i\omega_{3i}$ (this is the unstable case);

(iii) $D(K,\omega)=0$ has three simple, real roots ω_1, ω_2 and ω_5, and a double real root, $\omega_3=\omega_4\equiv\omega_{3r}$ (the marginal stability case).

The neutral stability curves, and sample solutions of the dispersion equation are described in Sec. 6.

Case (*i*) (*the stable case*). By inverting the transform solution for $\bar{a}_2(s,k)$ in (5.15), corresponding to the initial data (8.1), we obtain the solution for $a_2(x,t)$ in the form

$$a_2(x,t)=A_2\sum_{n=1}^{5}\Psi(K,\omega_n)\cos(\omega_n t-Kx), \tag{8.2}$$

where

$$\Psi(K,\omega_n)=\frac{N_2(K,\omega_n)}{D_\omega(K,\omega_n)} \tag{8.3}$$

and

$$N_2(k,\omega)=-i(\omega-k\lambda_1)(\omega-k\lambda_3)(\omega-k\lambda_5)(\omega-k\lambda_7), \tag{8.4}$$

and $D(k,\omega)$ is the dispersion function (5.14). From Sec. 6, the dispersion equation has five simple real roots if $0<k<k_L(\beta,\theta)$, or if $k>k_U(\beta,\theta)$, where $k=k_L$ and $k=k_U$ define the neutral stability surfaces.
From (5.21)–(5.24), the other wave amplitudes are given in terms of $a_2(x,t)$ by the formulae

$$a_4(x,t)=0, \tag{8.5}$$

$$a_j(x,t)=-\Lambda_{j2}\int_0^t dt'\; a_2(x-\lambda_j(t-t'),t'), \qquad j=1,3,5,7, \tag{8.6}$$

$$a_6(x,t)=\sum_{j\neq 2,4,6}\frac{\Lambda_{6j}\Lambda_{j2}}{\lambda_6-\lambda_j}\int_0^t dt'\int_{x-\lambda_6(t-t')}^{x-\lambda_j(t-t')}dx'\; a_2(x',t'). \tag{8.7}$$

It is straightforward to obtain closed form solutions for the wave amplitudes $\{a_j:1\leqslant j\leqslant 7,\ j\neq 2\}$ by using the solution (8.2) for $a_2(x,t)$ in (8.5)–(8.7) and carrying out the integrations.

Case (*ii*) (*the unstable case*). Inversion of the transform $\bar{a}_2(s,k)$ in (5.15) in this case yields the solution for $a_2(x,t)$ in the form

$$\begin{aligned}a_2(x,t)=A_2\Bigg(&\sum_{n=1,2,5}\Psi(K,\omega_n)\cos(\omega_n t-Kx)\\&+\exp(\omega_{3i}t)\,\mathrm{Re}\Big\{\Psi(K,\omega_3)\exp[-i(\omega_{3r}t-Kx)]\Big\}\\&+\exp(-\omega_{3i}t)\,\mathrm{Re}\Big\{\Psi(K,\omega_3)\exp[i(\omega_{3r}t-Kx)]\Big\}\Bigg).\end{aligned} \tag{8.8}$$

https://doi.org/10.1017/S0022377801001283 Published online by Cambridge University Press

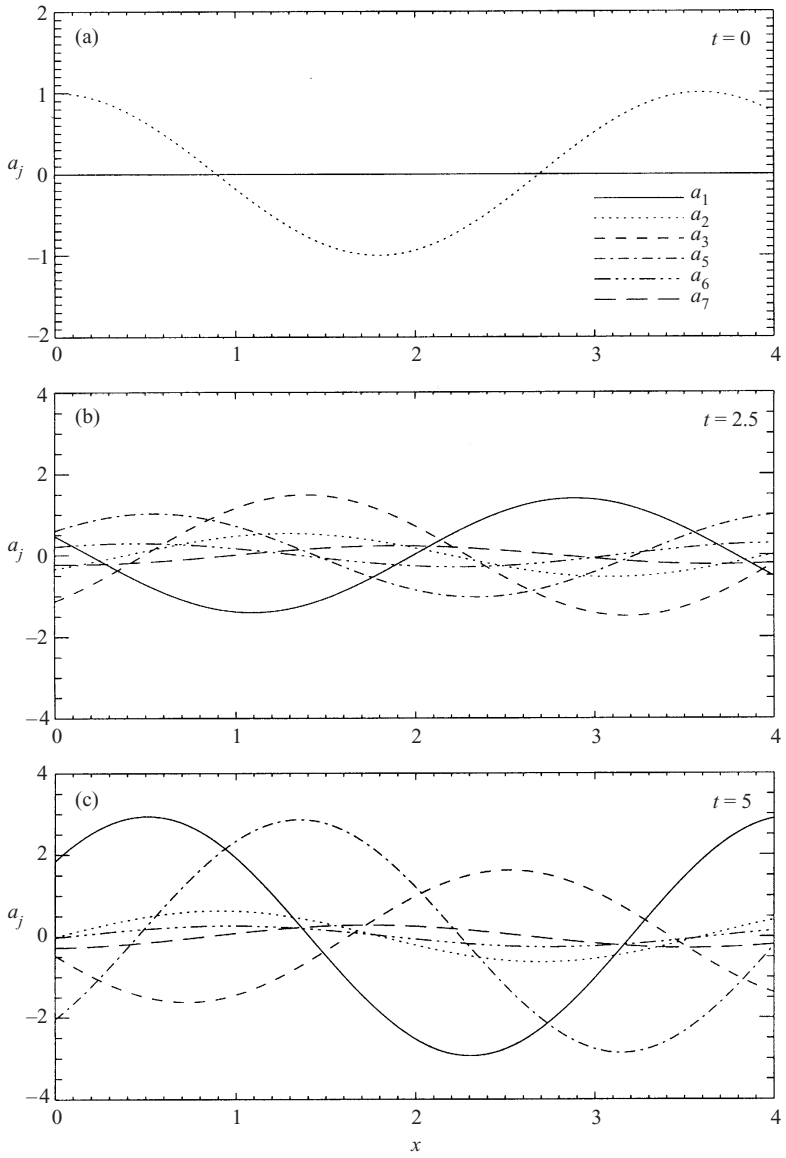


Figure 10. Solutions of the wave mixing equations (8.5)–(8.8) for an unstable case with periodic initial data $a_2(x,0)$ and with $a_j = 0$ at $t = 0$ for $j \neq 2$, described in (8.1). The parameters are $\beta = 0.1$ and $\theta = 30^\circ$ and $K = 1.75k_0$. The wave amplitudes $\{a_j(x,t) :\ 1 \leqslant j \leqslant 7,\ j \neq 4\}$ are shown at times $t = 0$, 2.5 and 5 in (a), (b) and (c) respectively.

Note that the solution (8.8) exhibits exponential growth with time, since $\omega_{3i} \neq 0$. The solutions for the other wave amplitudes are given in terms of $a_2(x,t)$ by (8.5)–(8.7).

Case (*iii*) (*the marginal stability case*). The solution for $a_2(x,t)$ in this case has the

https://doi.org/10.1017/S0022377801001283 Published online by Cambridge University Press

following form:

$$a_2(x,t) = A_2\left(\sum_{n=1,2,5} \Psi(K,\omega_n)\cos(\omega_n t - Kx) + 2\frac{N_{2\omega}(K,\omega_3)}{D_{\omega\omega}(K,\omega_3)}\cos(\omega_3 t - Kx)\right.$$
$$\left. -2\frac{N_2(K,\omega_3)}{D_{\omega\omega}(K,\omega_3)} t\sin(\omega_3 t - Kx)\right). \tag{8.9}$$

Thus, in the marginally stable case, the solution for $a_2(x,t)$ exhibits secular wave growth due to the $t\sin(\omega_3 t - Kx)$ term in (8.9). The other wave amplitudes are given by (8.5)–(8.7).

Figure 10 shows an example of the solution (8.5)–(8.8) for the unstable case, with $\beta = 0.1$, $\theta = 30°$, $K = 1.75k_0$ and $A_2 = 1$. Initially, at time $t = 0$ (a), only the backward Alfvén mode is present. (b) and (c) show the solutions for the different wave modes at times $t = 2.5$ and $t = 5$ respectively. The growth rate $\omega_{3i} = 0.24878$ and $\omega_{3r} = 0.50306$. The backward and forward Alfvén waves (a_2 and a_6) and the forward fast mode wave a_7 are dominated by the other waves at time $t = 5$. From the structure of the wave mixing equations (4.3)–(4.9), this suggests that the wave mixing coefficients Λ_{2j}, Λ_{6j} $(j \neq 2,6)$, and the mixing coefficient Λ_{72} are small compared with the magnetoacoustic wave mixing coefficients Λ_{j2} $(j = 1,3,5,7)$. Hence a_2 mainly acts as the intermediary for the transfer of energy between the different modes. The forward Alfvén mode a_6 in this example can only be created by the two-step process in which a_2 transfers energy to a magnetoacoustic mode, followed by a transfer of energy from the magnetoacoustic mode to a_6 (see (8.7)).

8.2. Hump or pulse-like initial data

In this subsection, we consider the solution of the wave mixing equations (4.3)-(4.9) for initial data in which $a_2(x,0)$ is a single hump of the form

$$a_2(x,0) = \frac{\epsilon}{\pi(x^2+\epsilon^2)}, \qquad a_j(x,0) = 0 \qquad (j \neq 2). \tag{8.10}$$

Note that

$$a_2(x,0) \to \delta(x) \qquad \text{as} \qquad \epsilon \to 0. \tag{8.11}$$

Inverting the transform (5.15) for $\bar{a}_2(s,k)$ for the initial data (8.10) yields the solution for $a_2(x,t)$ as a double Fourier integral of the form

$$a_2(x,t) = \int_L \frac{d\omega}{2\pi}\int_F \frac{dk}{2\pi}\exp[i(kx-\omega t)]\frac{f(k,\omega)}{D(k,\omega)}, \tag{8.12}$$

where

$$f(k,\omega) = (\omega - k\lambda_1)(\omega - k\lambda_3)(\omega - k\lambda_5)(\omega - k\lambda_7)\hat{a}_2(k), \tag{8.13}$$

and

$$\hat{a}_2(k) = \int_{-\infty}^{\infty}\exp(-ikx)a_2(x,0)\,dx = \exp(-|k|\epsilon) \tag{8.14}$$

is the Fourier transform of the initial data $a_2(x,0)$. In (8.12), the contour F must lie in a strip of the complex k plane including the real k axis, where the integrand will be analytic for an appropriate choice of the contour L in the complex ω plane. The contour L is a straight line parallel to the real ω axis of the form $\omega = \omega_r + iL$, chosen so that there are no singularities of the integrand in $\mathrm{Im}(\omega) > L$ (this ensures that $a_2(x,t) = 0$ for $t < 0$).

https://doi.org/10.1017/S0022377801001283 Published online by Cambridge University Press

Briggs (1964), Bers (1983) and Brevdo (1988) considered similar initial value problems in wave stability problems. In the formulation of Bers (1983), the late-time asymptotics of the Green function

$$G(x,t) = \int_L \frac{d\omega}{2\pi} \int_F \frac{dk}{2\pi} \frac{\exp[i(kx-\omega t)]}{D(k,\omega)}, \tag{8.15}$$

was studied, where the contours L and F are described above. Bers (1983) reviews methods to determine whether the dominant instability in a plasma is a convective or absolute instability. These methods are used below to determine the late-time asymptotics of the solution (8.12). The definitions of absolute and convective instability are given below.

Definition 1. An *absolute instability* is one in which

$$\lim_{t\to\infty} G(x,t) \to \infty \tag{8.16}$$

for all x, where either x is fixed or $x = x_V(t)$ is the position of an observer moving with the growing envelope of G.

Definition 2. A *convective instability* is one for which

$$\lim_{t\to\infty} G(x,t) \to 0 \tag{8.17}$$

for a fixed finite x, and

$$\lim_{t\to\infty} G(x_V(t),t) \to \infty, \tag{8.18}$$

where the frame $x = x_V(t)$ moving with the growing envelope depends on $D(k,\omega)$ (Bers 1983).

To determine if the dominant instability for the solution (8.12) for $a_2(x,t)$ is an absolute instability, it is useful to rewrite the solution in the form

$$a_2(x,t) = \int_{\tilde{L}} \frac{d\omega}{2\pi} \exp(-i\omega t) I(x,\omega), \tag{8.19}$$

where

$$I(x,\omega) = \int_{\tilde{F}} \frac{dk}{2\pi} \exp(ikx) \frac{f(k,\omega)}{D(k,\omega)}. \tag{8.20}$$

The contours $\tilde{L}$ and $\tilde{F}$ in the complex ω and complex k planes are obtained by deforming the contours L and F in (8.12) in an appropriate manner. In particular, the contour $\tilde{L}$ can be deformed so that the roots of $D(k,\omega) = 0$ of the form $\omega = \omega(k_{\tilde{F}})$ (note that $k = k_{\tilde{F}}$ on the contour $\tilde{F}$) lie below the contour $\tilde{L}$ in the complex ω plane. This ensures that the causality constraint $G(x,t) = 0$ for $t < 0$ is satisfied. In order to evaluate the integral $I(x,\omega)$ in (8.20), we require that the roots of the dispersion equation $D(k,\omega) = 0$ for k as a function of ω split into two distinct sets of curves in the complex k plane, of the forms $k = k_u(\omega_L)$ and $k = k_l(\omega_L)$, where $\omega = \omega_L$ on the contour L. The $k = k_u(\omega_L)$ roots correspond to the $x > 0$ eigenmodes and the $k = k_l(\omega_L)$ roots correspond to the $x < 0$ eigenmodes. It is required that the curves $k = k_l(\omega_{\tilde{L}})$ lie below the deformed contour $\tilde{F}$, and that the curves $k = k_u(\omega_{\tilde{L}})$ lie above $\tilde{F}$ in the complex k plane. This ensures that the $x > 0$ eigenmodes and the $x < 0$ eigenmodes remain distinct, and unaffected by the contour deformation.

https://doi.org/10.1017/S0022377801001283 Published online by Cambridge University Press

A pinch point singularity occurs if there is a coalesence of a $k = k_u(\omega_{\tilde{L}})$ root with a $k = k_l(\omega_{\tilde{L}})$ root due to contour deformation, to form a double root of the dispersion equation $D(k, \omega) = 0$ for k. Such roots of the dispersion equation, $(k, \omega) = (k_p, \omega_p)$, pinch the deformed contour $\tilde{F}$ in the complex k plane at $k = k_p$, and touch the deformed contour $\tilde{L}$ at $\omega = \omega_p$ in the complex ω plane. The pinch point singularities (if they exist) in the simplest case imply

$$I(x, \omega) \propto \frac{\exp(ik_p x)}{(\omega - \omega_p)^{1/2}} \tag{8.21}$$

near the pinch point $\omega = \omega_p$. In this latter case, the most vigorous absolute instability arises from the pinch point $\omega = \omega_p$ that has the maximum imaginary part, and

$$\lim_{t\to\infty} G(x, t) \sim \frac{\exp[i(k_p x - \omega_p t)]}{t^{1/2}}, \tag{8.22}$$

for all x (Bers 1983).

Before proceeding to determine the possible pinch points, it is useful to note, for later reference, that use of the residue theorem in (8.20) yields

$$I(x, \omega_L) = i\left(H(x)\sum_{k_u^{(s)}} \frac{f(k_u^{(s)}, \omega_L)}{D_k(k_u^{(s)}, \omega_L)} \exp(ik_u^{(s)} x) - H(-x)\sum_{k_l^{(s)}} \frac{f(k_l^{(s)}, \omega_L)}{D_k(k_l^{(s)}, \omega_L)} \exp(ik_l^{(s)} x)\right), \tag{8.23}$$

where the superscript s labels the different roots $k_u(\omega_L)$ and $k_l(\omega_L)$, and $H(x)$ is the Heaviside step function. It is assumed in (8.23) that the roots of the dispersion equation are simple. This is in fact the case for our problem for an appropriate choice of the contour L, although the roots from the different branches can form a double root for $k(\omega_L)$ as the contour L is changed. Equations (8.19) and (8.23) show that $a_2(x, t)$ can be evaluated as a single Fourier integral (8.19) over ω, in which $I(x, \omega)$ is given by the residue sum (8.23) (this integral can also be expressed as an inverse Laplace transform if desired). The result (8.23) also plays an important role in the pinch point analysis of absolute instabilities (Bers 1983).

8.2.1. Pinch point analysis. The first step in determining the possible pinch points is to determine the double roots of the dispersion equation for $k = k(\omega)$ satisfying the simultaneous equations

$$D(k, \omega) = 0, \qquad \frac{\partial D(k, \omega)}{\partial k} = 0. \tag{8.24}$$

In the present application, the dispersion function $D(k, \omega)$ in (5.14) can be written in the form

$$D(k, \omega) = -i\omega_0^5[\bar{\omega}^5 \hat{D}(\chi) - \bar{\omega}^3 \hat{N}(\chi)], \tag{8.25}$$

where

$$\bar{\omega}^2 = \frac{\hat{N}(\chi)}{\hat{D}(\chi)} \tag{8.26}$$

is the form of the dispersion equation in (6.28), and $\chi = \bar{k}/\bar{\omega}$. Using (8.25) and (8.26), it follows that the dispersion equation has double roots for $k = k(\omega)$ when

$$\frac{\partial D(k, \omega)}{\partial \bar{k}} = \frac{i\omega_0^5 \hat{N}(\chi) P(\chi)}{\hat{D}(\chi)^2} = 0, \tag{8.27}$$

https://doi.org/10.1017/S0022377801001283 Published online by Cambridge University Press

Table 1. Double-root solutions of the dispersion equation satisfying $D(k,\omega) = D_k(k,\omega) = 0$ corresponding to the solutions of $P(\chi) = 0$, for the case $\beta = 0.1$ and $\theta = 60°$. The solutions of $P(\chi) = 0$ are $\chi = \chi_r + i\chi_i$, and the corresponding roots for k and ω are $k = k_r + ik_i$ and $\omega = \omega_r + i\omega_i$, where the subscripts r and i denote the real and imaginary parts. The index s denotes the root number.

s	χ_r	χ_i	ω_r	ω_i	k_r	k_i
1	0.585 36	0.000 00	1.199 5	0.000 00	0.702 15	0.000 00
2	−0.676 25	0.246 09	1.902 1	−1.822 9	−0.837 68	1.700 8
3	−0.676 25	−0.246 09	1.902 1	1.822 9	−0.836 78	−1.700 8
4	0.395 18	0.000 00	1.525 7	0.000 00	0.602 94	0.000 00
5	2.691 6	1.260 0	0.575 79	−0.367 39	2.012 7	−0.263 37
6	2.691 6	−1.260 0	0.575 79	0.367 39	2.012 7	0.263 37
7	−2.054 7	0.000 00	0.000 00	2.564 0	0.000 00	−5.268 2

where

$$P(\chi) = \hat{D}(\chi)\hat{N}'(\chi) - \hat{N}(\chi)\hat{D}'(\chi) \tag{8.28}$$

is a seventh-degree polynomial in χ.

Hence double-root solutions of $D(k,\omega) = 0$ for k can be obtained by determining the roots of the seventh-degree polynomial equation $P(\chi) = 0$. Equation (8.27) also has solutions for which $\hat{N}(\chi) = 0$, but these correspond to long-wavelength solutions of the dispersion equation of the form $\omega^{(j)} \simeq k\Lambda_j$, $j = 1, 2, 3$, which apply in the limit as $|k| \to 0$ (see Sec. 7). These solutions do not lead to instability, since $|k| \to 0$. Not all the seven roots of the polynomial equation $P(\chi) = 0$ are pinch points formed by the merging of two roots $k = k_l(\omega_{\tilde{L}})$ and $k = k_u(\omega_{\tilde{L}})$, associated with the $x < 0$ and $x > 0$ eigenmodes.

Since the polynomial $P(\chi)$ has real coefficients, its seven roots are either real or occur in complex-conjugate pairs. For a given solution for χ, say $\chi = \chi_s$, the corresponding solutions for $\bar{k}$ and $\bar{\omega}$ are given by the equations $\bar{\omega}_s^2 = \hat{N}(\chi_s)/\hat{D}(\chi_s)$ and $\bar{k}_s = \chi_s\omega_s$. Note that if (k_s, ω_s) is a solution for (k,ω), then $(-k_s, -\omega_s)$ is also a solution. This leads to 14 possible solution pairs for (k,ω).

Table 1 shows the seven roots of $P(\chi) = 0$ for the case $\beta = 0.1$ and $\theta = 60°$. There are three real roots for χ and two pairs of complex-conjugate roots. Only seven of the corresponding solutions for $k = k_r + ik_i$ and $\omega = \omega_r + i\omega_i$ are shown. There are seven more roots corresponding to $(-k, -\omega)$ not listed in the table.

Below we present evidence that case 6 in Table 1, with $\omega = \omega_p = 0.57579 + 0.36739i$ and $k = k_p = 2.0127 + 0.26337i$ is a pinch point, and that the point $(k,\omega) = (-k_p^*, -\omega_p^*)$ is also a pinch point, which implies that the instability is an absolute instability.

Figure 11 shows the dispersion equation solutions $k = k^{(\alpha)}(\omega_L)$ in the complex k plane for $L = 2.6$. There are three solution branches with $k_i < 0$, which correspond to the backward slow-mode wave (s_-), the backward Alfvén wave (a_-) and the backward fast-mode wave (f_-) as $|k| \to \infty$. These curves correspond to the $x < 0$ eigenmodes. Similarly, for $k_i > 0$, the curves correspond the forward fast mode (f_+) and the forward slow mode (s_+), and apply for $x > 0$. Note that none of the curves cross the real k axis, and hence the contour F in the Fourier integral (8.12) can be taken as the Re(k) axis. There are no double-root solutions for $k = k(\omega)$, where two solution branches intersect, because the double-root solutions have maximum $\omega_i = 2.564$ (case 7 in Table 1), which is less than L. Although the curve labelled

https://doi.org/10.1017/S0022377801001283 Published online by Cambridge University Press

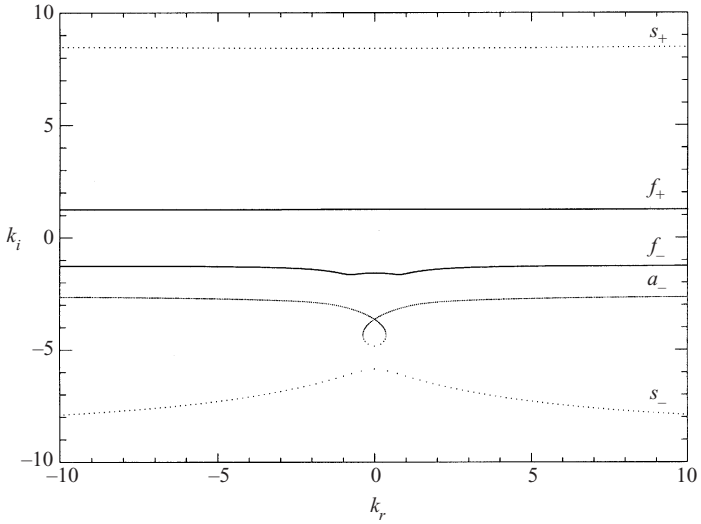


Figure 11. Solutions of the dispersion equation $D(k,\omega) = 0$ in the form $k = k^{(\alpha)}(\omega)$, $1 \leqslant \alpha \leqslant 5$, in the complex $k$plane, where $\omega = \omega_r + iL$, with $L = 2.6$. The parameters $\beta = 0.1$ and $\theta = 60°$. The curves labelled $f_\pm$, $s_\pm$, and a_- correspond to the backward and forward fast-mode waves, the backward and forward slow-mode waves, and the backward Alfvén wave, respectively.

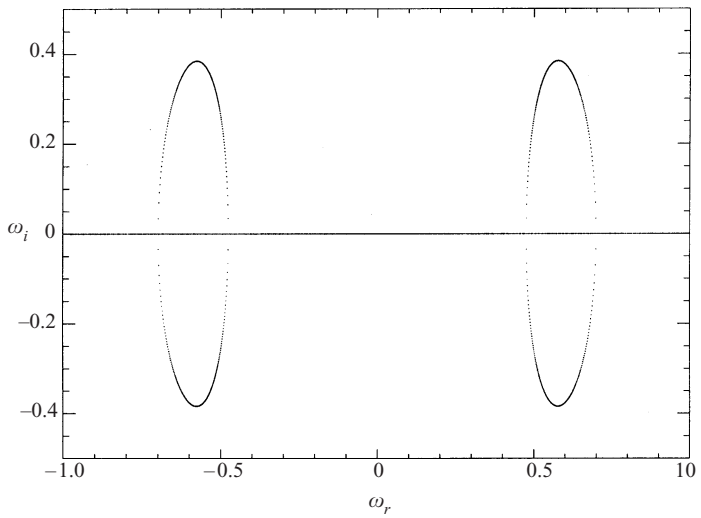


Figure 12. Solutions of the dispersion equation $D(k,\omega) = 0$ in the form $\omega = \omega^{(\alpha)}(k)$ in the complex ω plane, where $k = k_r$ is real, for the case $\beta = 0.1$ and $\theta = 60°$. In general, there are five real roots for ω, but two complex-conjugate roots and three real roots occur in the region $0.4756 < |\omega_r| < 0.6992$.

a_- loops back on itself, it is in fact a single-valued function of ω, and there are no double-root solutions for k associated with this curve.

Figure 12 shows solutions of the dispersion equation $D(k,\omega) = 0$ in the alternative form $\omega = \omega^{(\alpha)}(k_F)$ $(1 \leqslant \alpha \leqslant 5)$, where $k_F = k_r$ coincides with the Re(k) axis, for the case $\beta = 0.1$ and $\theta = 60°$. The figure shows that there is a complex-conjugate pair

https://doi.org/10.1017/S0022377801001283 Published online by Cambridge University Press

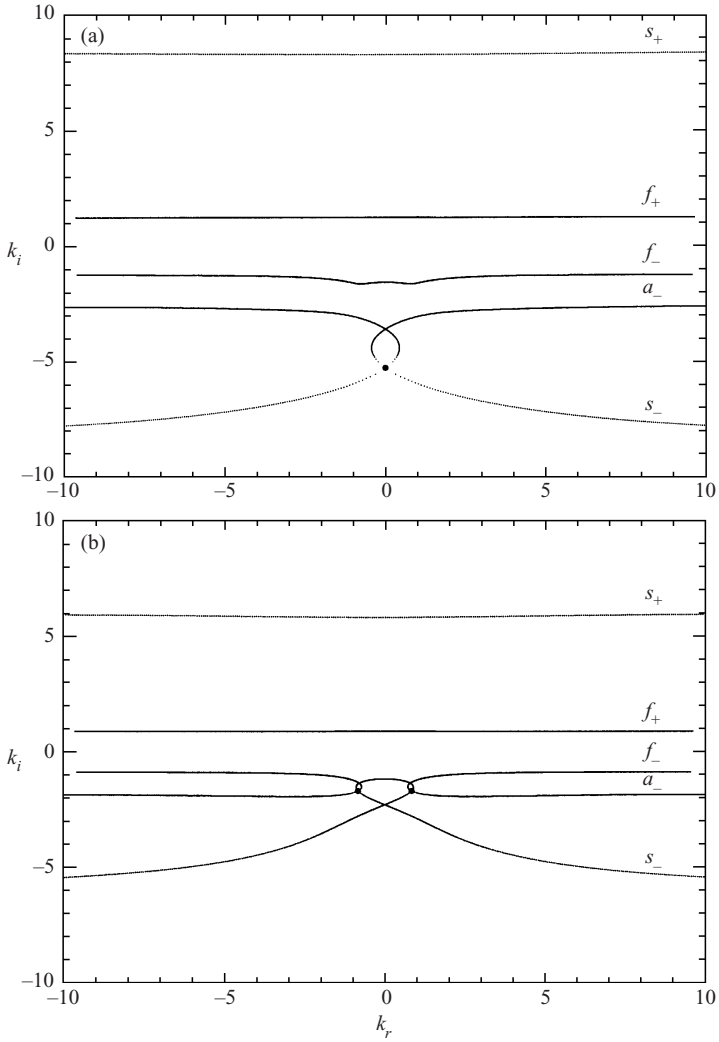


Figure 13. Dispersion equation solutions in the form $k = k^{(\alpha)}(\omega)$ $(1 \leqslant \alpha \leqslant 5)$, in the complex k-plane, where $\omega = \omega_r + iL$ for two values of L, and for the case $\beta = 0.1$ and $\theta = 60°$: (a) $L = 2.564$; (b) $L = 1.8229$. The bold dots mark double-root solutions for k.

of roots for $\omega_a < |\omega_r| < \omega_b$, where the frequencies $\bar{\omega}_a = 0.4756$ and $\bar{\omega}_b = 0.6992$ correspond to the neutral stability wavenumbers $\bar{k}_a = \bar{k}_U = 2.904$ and $\bar{k}_b = \bar{k}_L = 1.1768$ in Fig. 2. The other three roots for $\omega = \omega(k_r)$ in this wavenumber range (i.e. $k_L < |k_r| < k_U$) are real. The main point to note in Fig. 12 is that the choice $L > 0.3841$ (the maximum ω_i of the unstable roots) ensures that the causality constraint $a_2(x,t) = 0$ for $t < 0$ is satisfied.

Figures 13 and 14 show the effect of decreasing L on the dispersion equation solution curves $k = k^{(\alpha)}(\omega_{\tilde{L}})$ $(1 \leqslant \alpha \leqslant 5)$ in the complex k plane, for the case $\beta = 0.1$ and $\theta = 60°$. In Fig. 13(a), $L = 2.564$ corresponds to the double-root case 7 in Table 1. This point is located at $(k_r, k_i) = (0, -5.2682)$ and is marked by the bold dot. It is at the intersection of the s_- and a_- curves. This is not a pinch point, since both the s_- and a_- curves occur in the $\mathrm{Im}(k) < 0$ half-plane. In Fig. 13(b),

https://doi.org/10.1017/S0022377801001283 Published online by Cambridge University Press

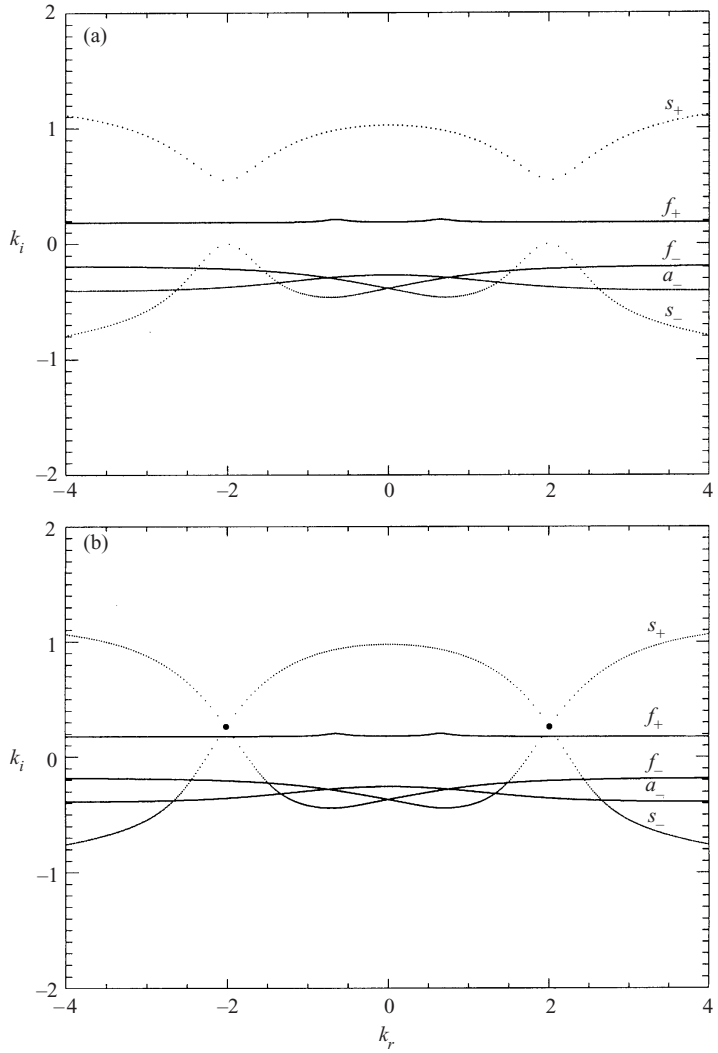


Figure 14. As Fig. 13, except that $L = 0.384\,11$ in (a) and $L = 0.3674$ in (b). In (a), the s_- solution curve just touches the Re(k) axis from below. In (b), with $L = 0.3674$, double-root solutions for k are marked by bold dots at the intersections of the s_- and s_+ curves. These pinch points imply the existence of an absolute instability.

L has been decreased to $L = 1.8229$. For this value of L, there are two double-root solutions for k (case 3 in Table 1), which are marked by bold dots and occur at the intersections of the a_- and f_- curves. These points are again not pinch points, since both the f_- and a_- curves lie in the $k_i < 0$ half-plane.

Figure 14(a) is for the case $L = 0.38411$. This corresponds to the maximum ω_i for the dispersion equation solution curves $\omega = \omega^{(\alpha)}(k_r)$ $(1 \leqslant \alpha \leqslant 5)$ in the complex ω plane displayed in Fig. 12. Notice that the backward slow-mode curves (s_-) have deformed to such an extent that they now just touch the Re(k) axis near $k_r = \pm 2$. For $L < 0.384\,11$, the backward slow-mode curve s_- pokes into the upper half k plane. It is then necessary to deform the Fourier contour F to $\tilde{F}$ for this mode, in order that the s_- curve lie below the deformed contour $\tilde{F}$. Figure

https://doi.org/10.1017/S0022377801001283 Published online by Cambridge University Press

14(b) is for $L = 0.367\,39$, which corresponds to the double-root case 6 in Table 1. This is a pinch point case, since the backward slow-mode curves s_-, originating in the $\mathrm{Im}(k) < 0$ half-plane at large $|k_r|$, now merge continuously with the s_+ curves in the $\mathrm{Im}(k) > 0$ half-plane. The curves meet at the double-root points $(k_r, k_i) = (\pm 2.0126\,74, 0.263\,37)$ and are marked by bold dots. The double-root points (the bold dots) lie above the forward fast-mode curve f_+. Thus it is necessary to use partial fractions to separate off the s_- and s_+ factors $k - k^{(1)}(\omega_{\tilde{L}})$ and $k - k^{(5)}(\omega_{\tilde{L}})$ in $D(k,\omega)$ in the Fourier integral (8.20) ($k^{(1)}$ and $k^{(5)}$ denote the s_- and s_+ modes respectively), and the deformed contour $\tilde{F}$ will be different for these two modes than for the other modes. It is then possible to have a deformed contour $\tilde{F}$ for the s_- and s_+ modes, which is pinched by the s_- and s_+ curves at the pinch points. Thus the instability is an absolute instability.

Following the analysis of Bers (1983), it follows that the late-time behaviour of $a_2(x,t)$ due to the two pinch points in Fig. 14(b) is

$$a_2(x,t) \simeq 2\frac{\exp(\omega_{pi}t - k_{pi}x)}{(\pi t)^{1/2}}\,\mathrm{Re}\left(\frac{f(k_p,\omega_p)\exp(i\phi)}{(D_{kk})_p(-2D_\omega/D_{kk})_p^{1/2}}\right), \tag{8.29}$$

where

$$\phi = k_{pr}x - \omega_{pr}t + \tfrac{1}{4}\pi. \tag{8.30}$$

In (8.29) and (8.30), $(k_{pr}, k_{pi}) = (2.0127, 0.263\,37)$ and $(\omega_{pr}, \omega_{pi}) = (0.575\,79, 0.367\,39)$ denote the locations of one of the pinch points in the complex k and complex ω planes. The other pinch point is located at $k = -k_p^*$ and $\omega = -\omega_p^*$.

8.2.2. Solution examples. From (8.19) and (8.20) it is straightforward to reduce the solution for $a_2(x,t)$ to the form

$$a_2(x,t) = \int_0^\infty \frac{d\omega_r}{\pi}\,\mathrm{Re}[\exp(-i\omega_r t + Lt)I(x,\omega_r + iL)], \tag{8.31}$$

where $\omega = \omega_r + iL$. Using the periodicity of $\exp(-i\omega_r t)$ with respect to ω_r, $a_2(x,t)$ can be approximated by

$$a_2^N(x,t) = \int_0^T \frac{d\omega_r}{\pi}\,\mathrm{Re}\left(\exp(-i\omega_r t)\sum_{j=1}^N \exp(Lt)I(x,\omega_r + (j-1)T + iL)\right), \tag{8.32}$$

where $T = 2\pi/t$ is the period of $\exp(-i\omega_r t)$ in ω_r. Effectively, $a_2^N(x,t)$ is the integral (8.31), with the upper limit of $\omega_r = \infty$ replaced by $\omega_r = NT$, which is a good approximation for a_2 for large enough N. Note that $I(x,\omega)$ can be evaluated using the residue sum (8.23).

Figure 15 illustrates the solution for $a_2(x,t)$, obtained by using the numerical approximation (8.32) with $N = 201$ and $L = 0.4$. The physical parameters used were $\beta = 0.1$, $\theta = 60°$ and the parameter $\epsilon = 0.1$ in the initial data (8.10). The figure shows the growth of $a_2(x,t)$ as t increases ($t = 0$, 4, 8, 12 and 16). Note that at each time t, there is an N-wave pulse propagating in the negative x direction at the Alfvén velocity $\bar{\lambda}_2 = -1$. This short-wavelength structure represents short-wavelength information in the initial pulse (the solid curve), which has not been substantially modified by wave–wave interactions. Note that at the later times $t = 12$ and $t = 16$, there is a substantial wave disturbance that fills up a larger region of position space as t increases (both for $x > 0$ and for $x < 0$), indicating the

https://doi.org/10.1017/S0022377801001283 Published online by Cambridge University Press

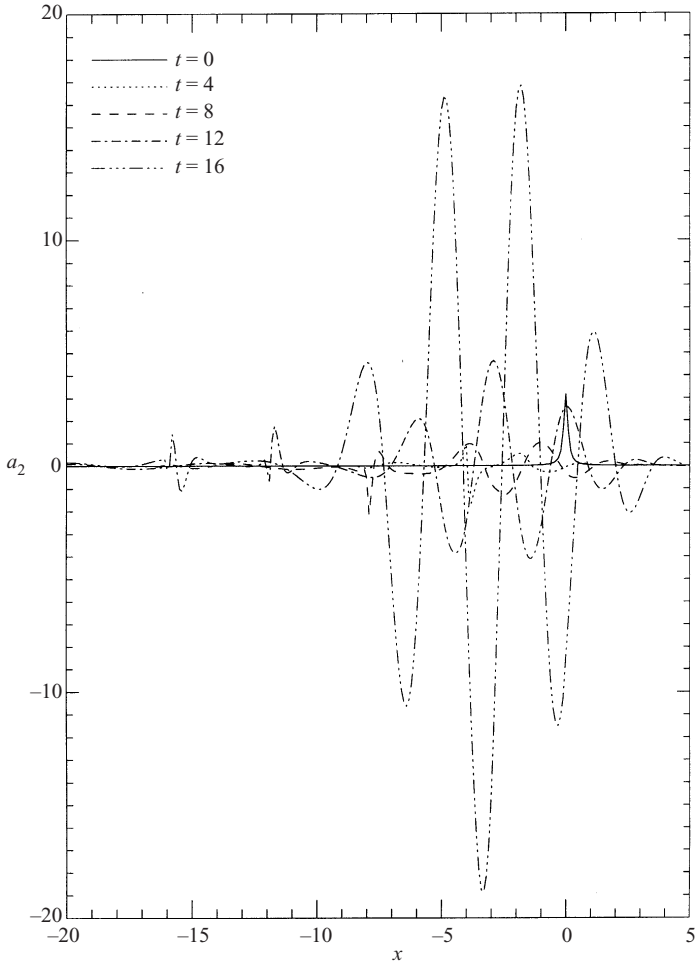


Figure 15. Solution for $a_2(x,t)$ calculated using the approximation (8.32) with $L = 0.4$ and $N = 201$. The physical parameters used were $\beta = 0.1$ and $\theta = 60°$. The initial data for $a_2(x,0)$ consists of the hump-like profile (8.10) with $\epsilon = 0.1$ and $a_j(x,0) = 0$ for $j \neq 2$. The figure shows the growth of an absolute instability in the system with increasing t ($t = 0$, 4, 8, 12 and 16).

presence of an absolute instability. To describe the short-wavelength characteristics of the solution accurately, it is necessary to determine the short-wavelength roots of the dispersion equation $D(k,\omega) = 0$ in the form $k = k^{(\alpha)}(\omega)$ ($1 \leqslant \alpha \leqslant 5$) that is needed in the evaluation of (8.32). For large ω_r (and large k_r), these roots are approximately given by

$$k^{(\alpha)} = \frac{\omega}{\lambda^{(\alpha)}} + \frac{\Gamma^{(\alpha)}}{\omega} + O\left(\frac{1}{\omega^2}\right), \tag{8.33}$$

where $1 \leqslant \alpha \leqslant 5$, $\lambda^{(\alpha)}$ is the appropriate wave speed and $\Gamma^{(\alpha)}$ is a constant. For example in the backward fast-mode branch solution of the dispersion equation, $\lambda^{(3)} = -c_f$ and $\Gamma^{(3)} = \Gamma_1$, where Γ_1 is given by (7.25).

Figure 16 shows a comparison of the 'exact' solution for $a_2(x,t)$ obtained by evaluating the integral (8.32) for $N = 201$ and $L = 0.4$ (denoted by a_{2e} in the

https://doi.org/10.1017/S0022377801001283 Published online by Cambridge University Press

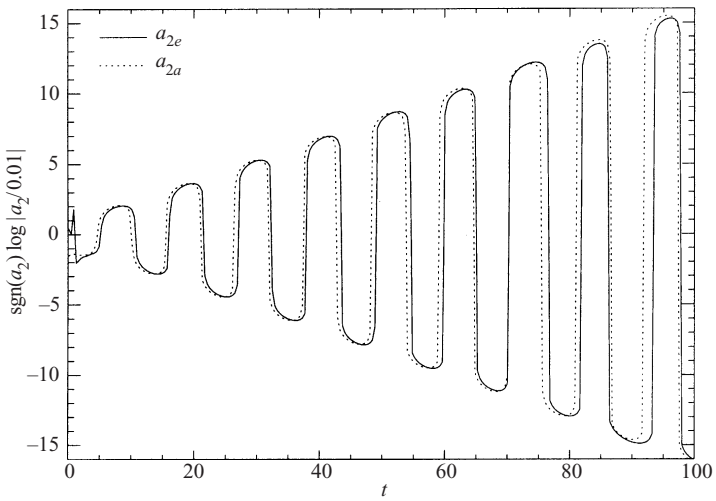


Figure 16. Comparison of the 'exact' solution approximation (8.32) for a_2 in the case $L = 0.4$ and $N = 201$ (labelled a_{2e}) with the pinch point approximation (8.29) (labelled a_{2a}) as a function of time t for $x = -1$. The parameters and the initial data are the same as in Fig. 15.

figure) with the asymptotic pinch point formula (8.29) for a_2 (labelled a_{2a}) as a function of t at $x = -1$, for the same physical parameters as in Fig. 15 (sgn(a_2) denotes the sign of a_2 on the ordinate axis). The figure verifies that the instability is an absolute instability, and shows that the pinch point approximation (8.29) roughly describes the growth of $a_2(x,t)$ with increasing t.

Formulae analogous to (8.31) and (8.32) for the other wave amplitudes $\{a_j(x,t) : j \neq 2\}$ can also be obtained using the results of Sec. 5. Figure 17 shows the wave amplitudes $\{a_j(x,t) : j = 1,2,3,5,6,7\}$ for the same initial data and physical parameters as in Fig. 15, at times $t = 0$, 8, 12, 16 (note $a_4 = 0$). The main point to note is the relative amplitude of the different eigenmodes. The slow modes (a_3 and a_5) have the largest amplitudes (a_5 is the largest), the Alfvén modes a_2 and a_6 are the next largest, and the smallest waves are the fast magnetoacoustic waves a_1 and a_7 ($|a_1| > |a_7|$). The fast modes a_1 and a_7 have extended precursors (for a_1, the precursor extends into $x < -20$, whereas for a_7, the precursor extends into $x > 5$ (not shown)), which is expected since the fast magnetoacoustic speed c_f is the largest short-wavelength speed in the system. The pinch point analysis (Fig. 14b) suggests that the slow modes a_3 and a_5 dominate the late-time behaviour.

9. Summary and discussion

The main aim of this paper has been to explore new aspects of the parametric instability of the large-amplitude, plane simple Alfvén wave studied by Goldstein (1978), Derby (1978) and Jayanti and Hollweg (1993b). The approach used by these authors was to obtain coupled second-order wave equations for sound waves and sideband Alfvén waves, with interactive source terms involving the pump Alfvén wave. In this development, the sound waves with wavenumber and frequency (k,ω) are generated by the interaction of the sideband Alfvén waves with wavenumbers and frequencies $(k \pm k_0, \omega \pm \omega_0)$ with the pump Alfvén wave with Fourier components

https://doi.org/10.1017/S0022377801001283 Published online by Cambridge University Press

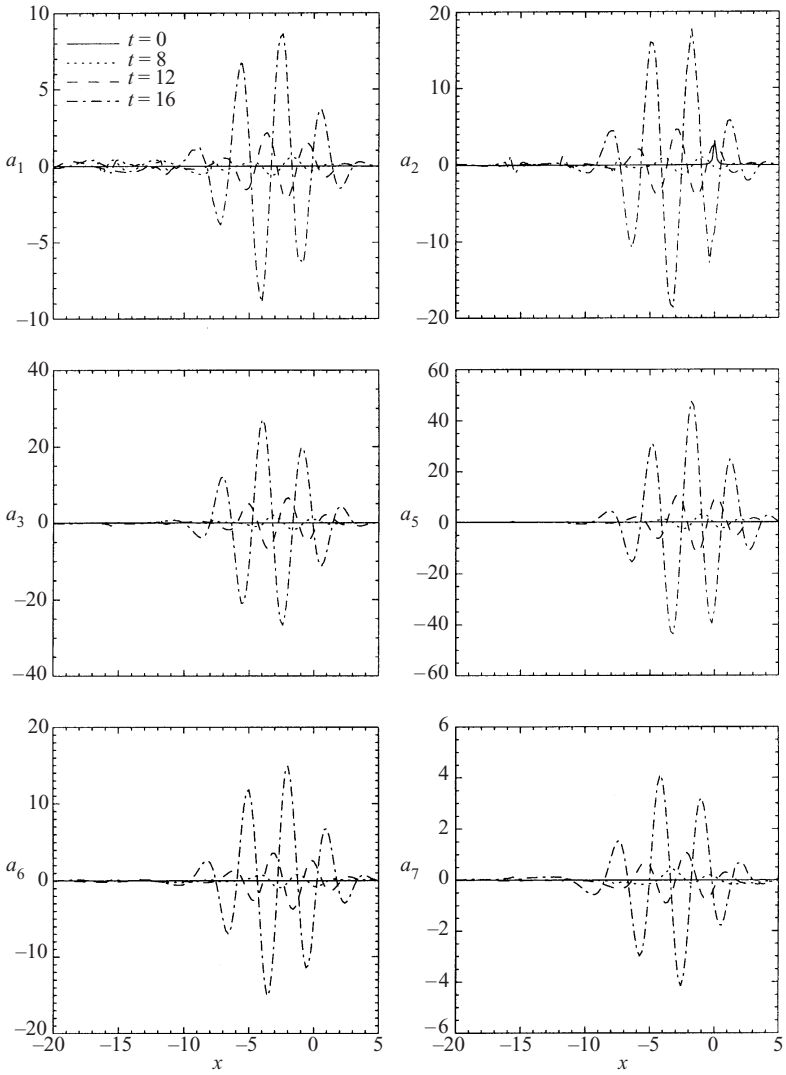


Figure 17. Wave amplitudes $\{a_j : j = 1, 2, 3, 5, 6, 7\}$ corresponding to the hump-like initial data (8.10), for the same initial data and physical parameters as in Fig. 15 ($\beta = 0.1$ and $\theta = 60°$). The wave amplitudes are shown at times $t = 0$, 8, 12 and 16.

at $(\pm k_0, \pm\omega_0)$. The sideband Alfvén waves in turn are generated by the interaction of the pump Alfvén wave with the sound waves (see also Sec. 4.2). The stability of the system depends on the solutions of the dispersion equation, which is a fifth-order polynomial equation in both k and ω.

The approach used in this paper relies on the wave mixing formalism for wave interactions in MHD in a non-uniform background flow developed by Webb et al. (1999). For MHD wave interactions in one Cartesian space dimension, the basic seven short-wavelength modes consist of the backward and forward fast and slow magnetoacoustic waves, the backward and forward Alfvén waves, and the entropy wave. In this approach, the large-amplitude pump Alfvén wave is regarded as the background flow, and the seven small-amplitude MHD waves interact with each

https://doi.org/10.1017/S0022377801001283 Published online by Cambridge University Press

other due to gradients and time dependence of the background flow. The formalism is similar to that used by Heinemann and Olbert (1980) and Zhou and Matthaeus (1990) to study the interaction of Alfvén waves and Alfvénic disturbances with the large-scale background solar wind flow. The wave mixing formalism can be used to study more general simple Alfvén waves, in which the wave amplitude depends on $\zeta = \zeta(\varphi)$, where ζ is an arbitrary differentiable function of the wave phase $\varphi = x - b_x t$, and in which the local scale length for the pump wave depends on the parameter $\eta = k_0 \zeta'(\varphi)$.

The form of the wave mixing equations (4.3)–(4.9) for the different wave amplitudes $\{a_j : 1 \leqslant j \leqslant 7\}$ (the short-wavelength MHD eigenvelocities are ordered so that $\lambda_{j+1} > \lambda_j$) shows that the backward Alfvén mode $a_2(x,t)$ acts as an intermediary that couples the magnetoacoustic waves (a_1, a_3, a_5 and a_7) with the pump wave, which propagates in the positive x direction.

Since the background flow is an Alfvén simple wave, it is natural to think of the wave mixing coefficient Λ_{js} as describing the interaction of wave s with the pump Alfvén wave, (wave 6), to produce a wave of type j. Using the results of Webb et al. (1999), one can show that

$$\Lambda_{js} = -\eta B_\perp \frac{\lambda_s - \lambda_6}{\lambda_s - \lambda_j} \Gamma_{js6} \qquad (\lambda_s \neq \lambda_j), \tag{9.1}$$

where

$$\Gamma_{jsp} = \mathbf{L}_j \cdot (\mathbf{R}_s \cdot \boldsymbol{\nabla}_{\boldsymbol{\psi}} \mathscr{A} \cdot \mathbf{R}_p) \tag{9.2}$$

is the three-wave interaction coefficient between wave s and wave p to produce wave j. In (9.1) and (9.2), $\mathscr{A}^{\alpha,\beta} = \partial F^\alpha / \partial \psi^\beta$ is the Jacobian matrix of the MHD fluxes $\{F^\alpha\}$ with respect to the conserved densities state vector $\boldsymbol{\psi} = (\rho, \rho\mathbf{u}^T, B_y, B_x, \rho S)^T$, and $\mathbf{R}_j$ and $\mathbf{L}_j$ are the orthonormal right- and left-eigenvectors of $\mathscr{A}^{\alpha,\beta}$. Thus, in the case where the background flow is one of the MHD simple waves, the wave mixing process can be regarded as a three-wave interaction process.

The general initial value problem for the wave mixing equations was studied in Sec. 5 by transform methods, for the case where the pump wave has constant wavenumber k_0 and frequency ω_0. The dispersion equation $D(k,\omega) = 0$ is the same as that obtained by Goldstein (1978), Derby (1978) and Jayanti and Hollweg (1993b). The backward Alfvén wave plays an important role in the coupling of the waves. For example, the solution for the magnetoacoustic waves $\{a_j(x,t) : j = 1,3,5,7\}$ in (5.24) consists of an initial value term $a_j(x - \lambda_j t, 0)$ propagated along the magnetoacoustic wave characteristic, plus a convolution term involving the interaction of the backward Alfvén wave with the pump wave. The forward Alfvén wave a_6 can be generated by a two-stage process, in which the backward Alfvén wave a_2 interacts with the pump wave to produce magnetoacoustic waves, and the magnetoacoustic waves interact with the pump wave to generate a_6. The solution for $a_2(x,t)$ can be expressed in terms of the Green function $G(x,t)$ for the system (see (5.24)–(5.26)) (cf. Bers 1983).

Solutions of the dispersion equation $D(k,\omega) = 0$ of the form (i) $\omega = \omega^{(\alpha)}(k)$ $(1 \leqslant \alpha \leqslant 5)$ for k real and (ii) $k = k^{(\alpha)}(\omega)$ for ω real were obtained. The solutions (i) admit unstable solutions in a restricted band of wavenumbers $k_L < k < k_U$, where the neutral stability curves $k = k_L(\beta,\theta)$ and $k = k_U(\beta,\theta)$ depend parametrically on the plasma β and on the pump wave amplitude $\delta = \tan\theta = B_\perp / B_x$ (Figs 2 and 3). This instability occurs at short wavelengths (i.e. at $k > k_L > k_0$), and has

https://doi.org/10.1017/S0022377801001283 Published online by Cambridge University Press

been investigated by previous authors. It is associated with the merging of the slow magnetoacoustic branches as k decreases (starting at $k = \infty$), and is a decay instability since it occurs at short wavelengths (Hollweg 1994). The wavenumber range for the instability decreases as the pump wave amplitude decreases (Fig. 3 shows that $k_U \to k_L$ as $\theta \to 0$). The growth rate ω_i increases as β decreases and as θ increases. The unstable modes of the form (ii) are spatially growing modes at a fixed frequency ω, and occur in the long-wavelength regime $0 < k < k_0$. These modes arise from the merging of the fast-mode wave branches at large ω or k. The instability occurs in the frequency range $\omega_0 < \omega_L < \omega < \omega_U < 2\omega_0$, where $\omega = \omega_L(\beta, \theta)$ and $\omega = \omega_U(\beta, \theta)$ are the neutral stability curves in the frequency domain. The growth rate k_i increases as β decreases and as θ increases ($0 < \theta < 90°$). Both types of solutions of the dispersion equation discussed above play an important role in distinguishing between amplifying and evanescent waves, and between convective and absolute instabilities (Sturrock 1958).

The wave mixing equations can be combined to yield a single master equation for the backward Alfvén wave perturbation $a_2(x, t)$ of the form

$$\mathscr{L}[a_2] = -\Lambda_{24}\mathscr{F}[a_4], \tag{9.3}$$

(7.1), in which the partial differential operator $\mathscr{L}(\partial_x, \partial_t) \equiv D(-i\partial_x, i\partial_t)$ is equivalent to the dispersion function $D(k, \omega)$ when the replacements $k \to -i\partial_x$ and $\omega \to i\partial_t$ are made. The source term $-\Lambda_{24}\mathscr{F}[a_4]$ in (9.3) is due to the entropy wave. The operator $\mathscr{L}$ is characterized by its long- and short-wavelength behaviour (Whitham 1959, 1974; Wu 1961). At long wavelengths ($k \to 0$), the dispersion equation to lowest order has solutions of the form

$$\omega^{(1)} = -2\omega_0, \qquad \omega^{(2)} = k\Lambda_1, \qquad \omega^{(3)} = k\Lambda_2, \qquad \omega^{(4)} = k\Lambda_3, \qquad \omega^{(5)} = 2\omega_0, \tag{9.4}$$

where $-c_f < \Lambda_1 < -c_s$, $c_s < \Lambda_2 < b_x$ and $b_x < \Lambda_3 < c_f$ (c_f and c_s denote the fast and slow magnetosonic speeds respectively). The results of Wu (1961) on the relative ordering of the long- and short-wavelength wave speeds imply that the waves are unstable in some finite wavenumber band $0 < k_L < k < k_U < \infty$. Expansion of the dispersion equation at long-wavelengths ($k \to 0$) yields the linearized Korteweg–deVries (KdV) equation (7.15) as the generic wave equation for the modes with $\omega^{(j+1)} = k\Lambda_j$ ($j = 1, 2, 3$) in (9.4) (these waves become the backward Alfvén wave and the backward and forward slow-mode branches at large k). The remaining modes $\omega^{(1)} = -2\omega_0$ and $\omega^{(5)} = 2\omega_0$ in (9.4) have infinite phase speeds $V_p^{(1)} = -2\omega_0/k$ and $V_p^{(5)} = 2\omega_0/k$ as $k \to 0$, and finite group velocity $V_g = -b_x$. These modes become the backward and forward fast-mode waves as $k \to \infty$. The dispersion equation expansion about $k = 0$ yields a version of the Schrödinger equation (7.22) for these waves. The dispersion coefficients in these equations are proportional to the square of the pump wave amplitude. We speculate that the weakly nonlinear generalizations of the equations are the nonlinear KdV equation and the nonlinear Schrödinger (NLS) equation.

It is of interest to enquire how the results of the pure MHD model differ from those of the Hall current plasma model. In the Hall plasma model (e.g. Wong and Goldstein 1986; Teraswa et al. 1986; Hollweg 1994), the detailed characteristics of the parametric instabilities depend on the polarization of the pump wave, the ion gyrofrequency $\mathbf{\Omega}_i$, the ion inertial length $\chi = b_x/\mathbf{\Omega}_i$, the pump wave amplitude $\delta = b_\perp/b_x$ and the plasma beta $\beta = a^2/b^2$. The MHD model applies at frequencies $\omega \ll \mathbf{\Omega}_i$ and at length scales $\ell \gg \chi$. The Hall plasma model allows for two different

https://doi.org/10.1017/S0022377801001283 Published online by Cambridge University Press

pump waves in the $x > 0$ direction, namely the left-hand-polarized (LHP) ion cyclotron wave and the right-hand-polarized (RHP) whistler wave (e.g. Terasawa et al. 1986). Both modes reduce to the Alfvén wave in the long-wavelength limit as $k \to 0$ and $\omega \to 0$. More complex models apply if electron inertial effects and the effects of minor ions are included in the analysis (e.g. Hollweg et al. 1993). Thus, for example, an expansion of the dispersion equation of Wong and Goldstein (1986) for one of the six daughter waves, about $k = 0$ for an LHP ion cyclotron pump wave propagating in the $x > 0$ direction, yields the Schrödinger equation

$$\left[i\left(\partial_t + \omega'(0)\partial_x\right) + \tfrac{1}{2}\omega''(0)\partial_x^2 - \omega(0)\right]\psi = 0, \tag{9.5}$$

for linear, long-wavelength waves, where

$$\left.\begin{aligned} \omega(0) &= -\frac{2\omega_0(1-\frac{1}{2}\omega_0/\Omega_i)}{1-\omega_0/\Omega_i}, \qquad \omega'(0) = -\frac{b_x}{(1-\omega_0/\Omega_i)^{1/2}(1-\frac{1}{2}\omega_0/\Omega_i)}, \\ \omega''(0) &= -\frac{2(1-\omega_0/\Omega_i)}{(1-\frac{1}{2}\omega_0/\Omega_i)^3}\left(\frac{b_\perp^2}{16\omega_0} + \frac{\chi b_x}{2}\frac{1-\frac{3}{4}\omega_0/\Omega_i}{1-\omega_0/\Omega_i}\right). \end{aligned}\right\} \tag{9.6}$$

The left-hand-polarized pump wave in (9.5) and (9.6) has frequency ω_0 and wavenumber k_0 satisfying the dispersion equation

$$\frac{\omega_0}{k_0 b_x} = \frac{1}{2}\sigma k_0\chi + \left(1 + \frac{1}{4}k_0^2\chi^2\right)^{1/2}, \tag{9.7}$$

with $\sigma = -1$ (note that for an RHP whistler wave as the pump wave, $\sigma = 1$). In the limit $\omega_0/\Omega_i \to 0$, the Schrödinger equation (9.5) reduces to the Schrödinger equation (7.22) for the pure MHD model (note that $\chi b_x \equiv (b_x^2/\omega_0)\omega_0/\Omega_i \to 0$ in this limit). In (9.6), the dispersion coefficient $D = \frac{1}{2}\omega''(0)$ has both a Hall current component $D \propto \frac{1}{2}\chi b_x$, which is the dispersion coefficient in the derivative nonlinear Schrödinger (DNLS) equation (e.g. Mjølhus 1976; Mio et al. 1976a,b), plus a further component $D \propto b_\perp^2/16\omega_0$ due to the interaction of the daughter waves with the pump wave (see also (7.22)). There are also sensitive dependences of the group velocity $V_g = \omega'(0)$ and the dispersion coefficient $D = \frac{1}{2}\omega''(0)$ on ω_0/Ω_i in the Hall plasma model. Similar Schrödinger equations or equations with KdV-type dispersion can be obtained for the other linear eigenmodes in the Hall plasma model. A Schrödinger equation for the pump wave can be obtained by expanding the pump wave dispersion equation (9.7) about $k_0 = 0$.

Note that we have not, in fact, derived the weakly nonlinear DNLS equation or the weakly nonlinear NLS equation describing wave modulation at long wavelengths. This requires the application of the method of multiple scales (reductive perturbation theory). Work is underway on the derivation of the NLS equation for the description of long-wavelength modulation of a linear carrier wave satisfying the wave mixing system (4.3)–(4.9).

Two initial value problems of the wave mixing equations were studied, in order to investigate the dependence of the wave stability on the initial data. The first problem illustrates the growth of the unstable waves for a case with periodic initial data, namely $a_2(x,0) = A\cos(Kx)$ and $a_j(x,0) = 0$ for $j \neq 2$, where K is a constant wavenumber. The solution depends on the roots $\omega = \omega^{(\alpha)}(K)$ $(1 \leqslant \alpha \leqslant 5)$ of the dispersion equation, and stable, unstable and marginally stable solutions forms were obtained. In the second problem, the initial data for $a_2(x,0)$ consisted of a single hump: $a_2(x,0) = \epsilon/[\pi(x^2+\epsilon^2)]$ and $a_j(x,0) = 0$ for the other wave modes (note that

https://doi.org/10.1017/S0022377801001283 Published online by Cambridge University Press

$a_2(x,0) \to \delta(x)$ as $\epsilon \to 0$). From the double-root solutions of the dispersion equation for k, satisfying the equations $D(k,\omega) = D_k(k,\omega) = 0$, it was established that an absolute instability develops at late time. The late-time asymptotic solution form for $a_2(x,t)$, (8.29), was obtained by using pinch point analysis (e.g. Bers 1983).

There are a variety of problems not addressed by the present paper. It is interesting to note that the quintic dispersion equation $D(k,\omega) = 0$ (in either ω or k) can be solved in terms of elliptic functions (see e.g. the discussion by McKean and Moll (1999), who refer to the original work by Hermite in 1859 on the quintic). Other problems not addressed in this paper include the questions of what equations govern weakly nonlinear waves in the system for the marginally stable cases and what is the detailed form of the weakly nonlinear equations governing the long-wavelength waves in the system. The wave mixing formalism used in this paper is applicable to systems with hyperbolic waves, but it is not clear how this approach can be used for dispersive waves, such as the Hall current plasma model investigated by Wong and Goldstein (1986), Terasawa et al. (1986), Hollweg (1994) and Vinas and Goldstein (1991a,b). Our work has been restricted to waves in one Cartesian space dimension. There is substantial interest in the development of Alfvén wave instabilities for multidimensional waves, including the filamentation instability (e.g. Passot et al. 1994; Champeaux et al. 1997a,b) not addressed in the present paper.

Acknowledgements

We acknowledge stimulating discussions with Thierry Passot on Alfvén wave instabilities, and some insightful remarks by one of the referees. The work of G.M.W. was supported in part by NASA Grant NAG5-5180. G.P.Z. is suppported in part at the BRI by NSF-DOE Award ATM-9713223, and in part by an NSF Young Investigator Award ATM 9357861.

References

Akhiezer, A. I., Akhiezer, I. A., Polovin, R. V., Sitenko, A. G. and Stepanov, K. N. 1975 *Plasma Electrodynamics*, Vol. 1. Oxford: Pergamon, Chap. 3.

Bers. A. 1983 Space–time evolution of plasma instabilities: absolute and convective. In: *Handbook of Plasma Physics*, Vol. 1 (ed. M.N. Rosenbluth and R.Z. Sagdeev). Amsterdam: North-Holland, p. 451.

Boillat, G. 1970 Simple waves in N-dimensional propagation. *J. Math. Phys.* **11**, 1482.

Brevdo, L. 1988 A study of absolute and convective instabilities with an application to the Eady model. *Geophys. Astrophys. Fluid Dyn.* **40**, 1.

Briggs, R. J. 1964 *Electron Stream Interaction with Plasmas*. Cambridge, MA: MIT Press.

Cabannes, H. 1970 *Theoretical Magnetofluiddynamics*. New York: Academic Press.

Champeaux, S., Passot, T. and Sulem, P. L. 1997a Alfvén-wave filamentation. *J. Plasma Phys.* **58**, 665.

Champeaux, S., Gazol, A., Passot, T. and Sulem, P. L. 1997b Plasma heating by Alfvén wave filamentation: a relevant mecahnism in the solar corona and the interstellar medium. *Astrophys. J.* **486**, 477.

Derby, N. F. 1978 Modulational instability of finite amplitude circularly polarized Alfvén waves. *Astrophys. J.* **224**, 1013.

Goldstein, M. L. 1978 An instability of finite amplitude circularly polarized Alfvén waves. *Astrophys. J.* **219**, 700.

Heinemann, M. and Olbert, S. 1980 Non-WKB Alfvén waves in the solar wind. *J. Geophys. Res.* **85**, 113.

Hollweg, J. V. 1994 Beat, modulational and decay instabilities of a circularly polarized Alfvén wave. *J. Geophys. Res.* **99**, 23 431.

https://doi.org/10.1017/S0022377801001283 Published online by Cambridge University Press

Hollweg, J. V., Esser, R. and Jayanti, V. 1993 Modulational and decay instabilities of Alfvén waves: effects of streaming He^{++}. *J. Geophys. Res.* **98**, 3491.

Hung, N. T. 1974 Parametric excitation of Alfvén and acoustic waves. *J. Plasma Phys.* **12**, 445.

Inhester, B. 1990 A drift kinetic treatment of the parametric decay of large amplitude Alfvén waves. *J. Geophys. Res.* **95**, 10 525.

Jayanti, V. and Hollweg, J. V. 1993a On the dispersion relations for parametric instabilities of parallel propagating Alfvén waves. *J. Geophys. Res.* **98**, 13 247.

Jayanti, V. and Hollweg, J. V. 1993b Parametric instabilities of parallel propagating Alfvén waves: some analytical results. *J. Geophys. Res.* **98**, 19 049.

McKean, H. P. and Moll, V. 1999 *Elliptic Curves*. Cambridge University Press.

Mio, J., Ogino. T., Minami, K. and Takeda, S. 1976a Modified nonlinear Schrödinger equation for Alfvén waves propagating along the magnetic field in cold plasmas. *J. Phys. Soc. Jpn* **41**, 265.

Mio, J., Ogino, T., Minami, K. and Takeda, S. 1976b Modulational instability and envelope solitons for nonlinear Alfvén waves propagating along the magnetic field in plasmas. *J. Phys. Soc. Jpn* **41**, 667.

Mjølhus, E. 1976 On the modulational instability of hydromagnetic waves parallel to the magnetic field. *J. Plasma Phys.* **16**, 321.

Passot, T. Sulem, C. and Sulem, P. L. 1994 Effect of longitudinal modulation on Alfvén wave filamentation. *Phys. Rev.* **E50**, 1427.

Sagdeev, R. Z. and Galeev, A. A. 1969 *Nonlinear Plasma Theory*. New York: Benjamin.

Sturrock, P. A. 1958 Kinematics of growing waves. *Phys. Rev.* **112**, 1488.

Swanson, D. G. 1989 *Plasma Waves*. San Diego: Academic Press.

Terasawa, T., Hoshino, M., Sakai, J. I. and Hada, T. 1986 Decay instability of finite amplitude, circularly polarized Alfvén waves: a numerical simulation of stimulated Brillouin scattering. *J. Geophys. Res.* **91**, 4171.

Vinas, A. F. and Goldstein, M. L. 1991a Parametric instabilities of circularly polarized large amplitude dispersive Alfvén waves: excitation of parallel propagating electromagnetic daughter waves. *J. Plasma Phys.* **46**, 107.

Vinas, A. F. and Goldstein, M. L. 1991b Parametric instabilities of circularly polarized large amplitude dispersive Alfvén waves: excitation of obliquely propagating daughter and side-band waves. *J. Plasma Phys.* **46**, 129.

Webb, G. M., Ratkiewicz, R., Brio, M. and Zank, G. P. 1996 Multi-dimensional MHD simple waves. *AIP Conf. Proc.* **382**, 335.

Webb, G. M., Brio, M., Zank, G. P. and Story, T. 1997 Wave–wave interactions in two-fluid cosmic-ray hydrodynamics. *J. Plasma Phys.* **57**, 631.

Webb, G. M., Ratkiewicz, R., Brio, M. and Zank, G. P. 1998 Multidimensional simple waves in gas dynamics. *J. Plasma Phys.* **59**, 417.

Webb, G. M., Zakharian, A. R., Brio, M. and Zank, G. P. 1999 Wave interactions in magnetohydrodynamics and cosmic-ray-modified shocks. *J. Plasma Phys.* **61**, 295.

Webb, G. M., Zakharian, A. R., Brio, M. and Zank, G. P. 2000 Nonlinear and three-wave resonant interactions in magnetohydrodynamics. *J. Plasma Phys.* **63**, 393.

Whitham, G. B. 1959 Some comments on wave propagation and shock wave structure with application to magnetohydrodynamics. *Commun. Pure Appl. Math.* **12**, 113.

Whitham, G. B. 1974 *Linear and Nonlinear Waves*. New York: Wiley.

Wong, H. K. and Goldstein, M. L. 1986 Parametric instabilities of circularly polarized Alfvén waves including dispersion. *J. Geophys. Res.* **91**, 5617.

Wu, T. T. 1961 A note on the stability condition for certain wave propagation problems. *Commun. Pure Appl. Maths* **54**, 745.

Zhou, Y. and Matthaeus, W. H. 1990 Transport and turbulence modeling of solar wind fluctuations. *J. Geophys. Res.* **95**, 10 291.

https://doi.org/10.1017/S0022377801001283 Published online by Cambridge University Press